Evaluation of weak intermolecular interactions in molecular crystals *via* experimental and theoretical charge densities

PARTHAPRATIM MUNSHI and TAYUR N. GURU ROW*

Solid State and Structural Chemistry Unit, Indian Institute of Science,
Bangalore-560012, India

Analysis of charge density distributions in molecular crystals has received considerable attention in the last decade both from high-resolution X-ray diffraction studies and from high-level theoretical calculations. An overview of the progress made in deriving one-electron properties, intermolecular interactions in terms of the Atoms in Molecule (AIM) approach (R.F.W. Bader. *Atoms in Molecules-A Quantum Theory*, Clarendon, Oxford (1990), R.F.W. Bader. *J. Phys. Chem.*, **A102**, 7314 (1998)) is given with special emphasis on improvements in charge density models and development of both experimental and theoretical techniques to interpret and analyse the nature of weak intermolecular interactions. The significance of the derived results from the charge density of coumarin and its derivatives have been analysed to obtain insights into the nature of intermolecular $C-H \cdots O$, $C-H \cdots \pi$, $\pi \cdots \pi$, $C-H \cdots S$, and $S \cdots S$ contacts. The appearance of a 'region of overlap' to segregate hydrogen bonds from van der Waals interactions based on the criteria proposed by Koch and Popelier (U. Koch, P.L.A. Popelier. *J. Phys. Chem.*, **99**, 9747 (1995), P.L.A. Popelier. *Atoms in Molecules. An Introduction*, pp. 150–153, Prentice Hall, UK (2000)) and the identification of differences in energy surfaces in concomitant polymorphs of 3-acetylcoumarin are described.

Keywords: X-ray diffraction; Charge density; *ab initio* theory; Intermolecular interactions; Crystal engineering; Hydrogen bond limit

Contents

*Corresponding author. Fax: +91-80-23601310. Tel.: +91-80-22932796. Email: ssctng@sscu.iisc.ernet.in

1. Introduction

1.1. *General*

Measurement of charge densities using high-resolution single crystal X-ray diffraction data of molecular crystals has now reached a level at which highly reliable theoretical measures can be compared. This has become possible particularly with the advances made in the experimental techniques, measuring devices, and high-speed computation. Of these, advances made in new area detectors, such as image plates (IP) and charge coupled devices (CCD), stand out as a major boost for rapid accumulation of extremely accurate data sets. Several recent reviews and articles comprising developments in both experiment and theory highlight the importance of mapping electron densities to deduce structure–property correlations [1–8]. Designing new solids with desirable physical and chemical properties has been the main motivation of chemists in recent times and the emphasis is on the synthesis of representative model compounds to generate required packing modes of molecular species in a crystalline framework. The understanding of intermolecular interactions, the so-called elements of crystal engineering [9], is of paramount significance in this context. In their review on 'Chemical applications of X-ray charge density analysis', Koritsánszky and Coppens [1] concluded that 'X-ray charge density analysis has grown into a mature field and, like in the development of structure determination, the methods have been standardized to a large extent so that more routine use becomes possible.' Further they observed that parallel analysis of theoretical results on both isolated molecules and periodic crystals is becoming common and molecular properties, which change upon incorporation of the molecule into a solid, can be analysed. Using Hirshfeld surfaces to partition crystal space, McKinnon *et al.* [10] have demonstrated a new methodology of exploring packing modes and intermolecular interactions in molecular crystals. This provides, apart from a visual picture of types of interactions present, a quantitative measure in terms of relative strengths involved in holding molecular species together in a crystalline lattice. The emphasis of the present review mainly concentrates on the evaluation and characterization of weak intermolecular interactions in terms of both experimental and theoretical charge-density analysis.

Since X-rays are almost exclusively scattered by electrons, the use of X-ray diffraction techniques for mapping the charge density distribution in crystals is an obvious choice. The advent of high speed computers together with technological developments in accumulating highly accurate X-ray diffraction data in quick time has made this possible to levels at which the best theoretical charge density calculations can be compared [11]. It is noteworthy that crystallographic experiments also allow for the identification of intermolecular interactions and, with accurate data sets followed by a charge density mapping, information on charge transfer in co-crystals with different molecular components can be analysed [12,13]. Experimental data sets are generally evaluated to account for the deformation densities due to chemical bonding by using Hansen and Coppens formalism [14] incorporated in the package XD [15]. Multipole refinements of experimental structure factors followed by topological analysis of the derived electron density and evaluation of the atomic basin properties results in the calculation of one-electron properties. Quantum chemical calculations have been demonstrated to generate accurate wavefunctions for chemically interesting species. Several powerful computer programs, e.g. GAUSSIAN [16], have been developed over the last few years, which provide high level *ab initio* wavefunctions for a fairly complex molecule without much effort. The advantage one gains in obtaining charge density distributions from experimental methods despite considerable effort and time is the automatic incorporation of correlated motion of electrons, a feature, which is generally neglected in theoretical calculations, e.g. the Hartree–Fock (HF) method. Of late, the practice has been to carry out the experimental and theoretical charge density studies in parallel providing a one-to-one comparison at various levels of accuracy. In this context the development of the program package CRYSTAL03 [17], which allows one to perform the single point periodic calculations based on a given geometry using different methods, e.g. HF or density functional theory (DFT) with high level basis sets, has been of enormous utility. This program provides the option to perform theoretical calculations keeping the lattice features (possible space groups) intact, thus facilitating structural features to be mimicked in all calculations.

The density-based quantum theory of Atoms In Molecules (AIM) [18,19] has established as the most powerful tool to analyse and interpret the charge densities obtained from both experiment and theory. This buffer zone technique also provides a platform to quantify the results in terms of one-electron properties that can be derived from the charge density distribution in the crystal. The identification of critical points (CP) where the gradient of the electron density vanishes, the mapping of bond paths (BP), which trace the inter-nuclear distance, the Laplacian of the electron density, which brings out the nature of intra and intermolecular interactions are some of the components resulting from the AIM analysis.

Evaluation of weak interactions has become an area of enormous interest since it provides the basis for supramolecular aggregation. With the identification of hydrogen bonds, which display stabilization energies to varying degrees in a crystalline lattice, the application of topological analysis to decipher the nature of such bonds has attracted considerable attention. In order to characterize weak and strong hydrogen bonds and to distinguish these from pure van der Waals interactions in terms of specific properties like bond order, ionicity, and conjugation, Koch and Popelier (hereinafter referred to as KP) [20,21] have proposed eight criteria. These criteria establish the formation of hydrogen bonds on a

quantum basis. The importance of this feature will become more evident later during the review.

1.2. *Definition of intermolecular interactions, crystal engineering*

One of the most significant factors in molecular crystals is the optimized arrangement of molecules in the crystal lattice. This is achieved by a subtle interplay of molecular recognition on one hand and the symmetry present in the lattice on the other. It is the ambition of a crystal engineer to unravel the nature of such balance of interactions between component molecules in the crystal. Intermolecular interactions of varying strengths have been identified to provide best choices for optimized packing in the environment governed by symmetry restraints in a crystalline lattice. In the last three decades, systematics based on results derived from the Cambridge Structural Database (CSD Version 5.26, November 2004 and one update in February 2005) [22,23] have generated several well-identified patterns, called synthons [24–26], serving as the basic tools in crystal engineering. Indeed, the area of crystal engineering has emerged as a major component in chemical crystallography and its impact is felt with the introduction of three specialized journals, *Crystal Growth and Design*, *Crystal Engineering Communications*, and *Crystal Engineering*, dedicated to report progress in this area.

Hydrogen bonds have been the most widely studied among all intermolecular interactions, however, a clear and unequivocal understanding is yet to be reached. A working definition has emerged very recently [27], which states '*A hydrogen bond exists between X−H and an atom (or group of atoms) A, if the interaction between X−H and A (1) is bonding and (2) sterically involves the hydrogen bond*.' It is noteworthy that the definition of this kind is fairly general and defines both strong and weak H-bonds. Further, the directional dependence of such interactions is also incorporated. Among the crystallographic community an H-bond is defined in terms of a distance-angle criterion [9,27–29] incorporating the directional preferences and a distance cut-off (less than the sum of the van der Waals radii of the participating atoms H and A). The major concern in such a definition comes from the fact that strong H-bonds have nearly covalent interactions while weaker H-bonds are generally electrostatic in nature. In fact, there has been no experimental proof for a critical distance at which the H-bond switches to van der Waals type. Koch and Popelier have proposed eight criteria, which need be satisfied to conclude the formation of a H-bond based on theoretical charge density distributions between H and A [20,21]. A possible 'region of overlap', which allows for the switching from an H-bond to van der Waals type has been identified, based on the charge density analysis of coumarin and two of its derivatives from both experiment and theory [30]. This finding, if explored and extended to all molecular crystals, might eventually serve as a definition to evaluate the nature of interactions and classification of weak and strong H-bonds.

Crystal engineering has clearly brought out the importance of recognizing patterns found by intermolecular interactions. For H-bonds, several approaches have been suggested and the method of Etter [31] has paved the way for characterizing H-bonds in terms of predefined motifs like ribbons, tapes, and loops. The approach to use CSD to view intermolecular interactions, e.g. H-bond parameters in terms of crystal correlations studies, has come to be recognized as a powerful tool to gain insights into weak and strong H-bonds [22,23,32,33]. It is the intention of this

review to give proper weighting to the derived crystal engineerig tools in terms of crystal correlation studies by combining the results obtained from charge density analysis in terms of CPs, BPs, and the Laplacian in intermolecular space. This *quantitative crystal engineering* would allow for a unique evaluation of weak intermolecular interactions in molecular crystals.

1.3. *Elements of electron density determination*

The basis of X-ray structure analysis is the assumption that the atomic electron density is essentially the spherically averaged density of an isolated atom. This allows for considering the molecular crystal to be built up by spherical independent atoms, which bond together into a molecule, which then rearranges following the allowed symmetry in the crystal lattice as a molecular crystal. The independent atom model (IAM) also assumes that the atoms in a crystal are neutral. The success of the spherical atom model has been witnessed in terms of the large number of crystal structures that have been determined based on this assumption.

$$\rho_{\text{IAM}}(\mathbf{r}) = \sum_k \rho_k^0(\mathbf{r} - \mathbf{R}_k)$$

This equation retains the electrons localized around a nucleus and further assumes that the electron density in the molecule (and eventually in the crystal) is a superposition of isolated spherical densities ρ^0 of isolated atoms k centered at $\mathbf{R}_k$. In general, diffraction is a phenomenon, which keeps the average density $\langle \rho \rangle$ as a canonical ensemble, which allows for thermal averaging as well. The thermal smearing is again restricted to the atom center and the mean square atomic displacement is expressed in terms of either harmonic or anharmonic parameters. Further, the Fourier transform leads to the generalized structure factors,

$$F(\mathbf{H}) = \sum_k f_k(\mathbf{H}) \exp(2\pi^2 \mathbf{H}^t \mathbf{U}_k \mathbf{H}) \exp(2\pi i \mathbf{H} \mathbf{R}_k^0)$$

The IAM is effective for heavy atoms with dominant core scattering, while for light atoms the directional characteristics in terms of bonding features like valence becomes more and more aspherical. This results in properties exhibited by molecular crystals such as the dipole moment and higher electrostatic moments. The limitations of IAM are not adequate to describe the scattering from covalently bonded crystals, e.g. in diamond the appearance of the space-group forbidden 222 reflection and the anomalously high intensity of the 100 reflection in the powder diffraction pattern of graphite. Further, theoretical and experimental evidence showing that atoms in molecules carry partial charges necessitated improvements over the IAM. The first extension of IAM to allow for both valence charge transfer and expansion/contraction of the valence shell was suggested by Coppens *et al.* [34], now called a radial (kappa, κ) refinement strategy. Various groups introduced several aspherical correction terms, [35,36] but the multipole expansion model suggested by Hansen and Coppens [14] has stood the test of time and is now the most widely used methodology. In their model, the individual atomic densities are divided into three components, the core,

spherical expansion and contraction term (κ) in the valence shell and the valence deformation in terms of density normalized spherical harmonics ($d_{lm\pm}$) together with the corresponding radial expansion and contraction (κ') of the valence shell as given below,

$$\rho_{\text{at}}(\mathbf{r}) = \rho_{\text{core}}(\mathbf{r}) + P_v\kappa^3\rho_{\text{valence}}(\kappa\mathbf{r}) + \sum_{l=0}^{l_{\text{max}}}\kappa'^3 R_l(\kappa'\mathbf{r})\sum_{m=0}^{l}P_{lm\pm}d_{lm\pm}(\vartheta,\varphi)$$

where the core (ρ_{core}) and spherical valence (ρ_{valence}) densities can be calculated from HF or relativistic HF atomic wave functions, while the radial function, $R_l(\kappa'\mathbf{r})$ of the deformation density takes the form of normalized Slater (or Gaussian) functions. The total electron density distribution is calculated based on F(H), the structure factor, by the Fourier transformation as

$$\rho(\mathbf{r}) = \int F(\mathbf{H})\exp(-2\pi i\mathbf{H}\cdot\mathbf{r})d\mathbf{H}$$

The difference $\Delta\rho$ between the observed and the calculated electron density is called *residual density*. This is a representation of the inadequacy of the multipolar modeling and is evaluated as follows

$$\Delta\rho(\mathbf{r}) = \rho_{\text{obs}}(\mathbf{r})-\rho_{\text{calc}}(\mathbf{r}) = \frac{1}{V}\sum_{H}\Delta F\exp(-2\pi i\mathbf{H}\cdot\mathbf{r})$$

The *deformation* density [1,37], the difference between the total density and the density calculated based on the *promolecule* density is a representation of valence density into the bonding regions and can be expressed as

$$\Delta\rho(\mathbf{r}) = \rho(\mathbf{r})-\rho_{\text{pro}}(\mathbf{r})$$

If the observed structure factors are used, the resulting electron density map is called a *dynamic deformation density* map, since the observed structure factors include thermal effects. The *static deformation density* map is free from thermal smearing effects and can be directly compared with theoretical deformation density.

2. Intermolecular interactions

Understanding and rationalization of crystal structures stands out from a basic understanding of the nature of molecular interactions, which provide pathways for recognition and packing in the lattice. The link between the molecule and the crystal originates from the intermolecular space and the interactions therein. Intermolecular interactions are of enormous importance because they provide for the energy minimization in the framework restricted by crystal symmetry. In this context, H-bonds play a major role and cover the entire energy range between covalent bonds and van der Waals interactions. Interactions involving halogens, sulfur, and selenium also

provide well-defined directionality to pack molecules in the crystal lattice [28]. Analyses of intermolecular interactions resulting in organized flexible/rigid frameworks provide pointers to the design of futuristic materials [38]. It is of interest to note that researchers in several areas zoom in on the features of intermolecular interactions as they provide useful guidelines for structure–activity correlations [39].

2.1. *Strong and weak hydrogen bonds*

Several exhaustive reviews, books, and articles on H-bonds are available in the literature [27 and the references therein, 9,28,29,31,40] and we shall restrict attention mainly to the classification of H-bonds, the nature of the H-bonds, and their limits. H-bonds can be classified as very strong, strong, and weak [28]. These are essentially differentiated based on geometrical, energetic, and thermodynamic features. In its strongest bonding environment (bond energy 15–40 kcal/mol), like for example in $O-H \cdots O$ with an $O \cdots O$ distance of 2.2 to 2.5 Å, the bond lengths $H \cdots O$ and $O-H$ are nearly the same and the geometry of $O-H \cdots O$ is nearly 180°. These demonstrate pronounced covalency and generate rigid frameworks. In H-bonds with donor (D) to acceptor (A) distance in the range 2.5–3.2 Å (e.g. H-bonds of the type $O-H \cdots O$, $N-H \cdots O$, $N-H \cdots S$, and $N-H \cdots N$) with bond energies ranging 4–15 kcal/mole, the interactions are mainly electrostatic with almost all bonds shorter than the sum of the van der Waals radii. The ability of a $C-H$ group to act as a proton donor depends on the hybridization at the C-atom site along with the presence of electron-withdrawing groups in the adjacent sites. The H-bonds generated are in the *weak* category e.g. $C-H \cdots O$ [28 and the references therein], $C-H \cdots N$ [41], $C-H \cdots F$ [42,43], $C-H \cdots Se$ [44]. The effect of these interactions on crystal packing is not as pronounced but a collective effect is often seen to introduce moderate charge effects suggesting variants in crystal engineering. A path-breaking charge-density-based analysis, to categorize strong and weak H-bonds, has been reported recently by Mallinson *et al.* [45], which indicates 'a Morse-like dependence of the Laplacian of $\rho(\mathbf{r})$ on the length of interaction line, which allows a differentiation of ionic and covalent bond characters'. The strength of the interactions studied varies systematically with the relative penetration of the CPs into the van der Waals spheres of the donor and acceptor atoms, as well as on the interpenetration of the van der Waals spheres themselves. This by far has been the most complete description of the continuum 'from weak interactions to covalent bonds' reported in the literature.

2.2. *Interactions involving sulfur and results from database analysis*

Intermolecular interactions involving sulfur have been studied extensively from the very early days of vibrational spectroscopy [46] to modern day charge density analysis [30,47,48]. It is of interest to note that the S-atom is in the third row of the periodic table and has available *d* orbitals for bonding. The interest stems from the nature of the S-atom, when it is found as $S-H$ because of its abundant occurrence in many biological and chemical systems. It is expected that the hydrogen bonding, as in the case of the $O-H$ group, could be cooperative resulting in the S-atom being both an acceptor and a donor. Thus the $S-H$ group may simultaneously act to generate complex H-bonded networks in crystal structures. Also it has been suggested by Desiraju and Steiner in their book on 'The weak hydrogen bond: In structural

Table 1. Statistical detail of the occurrence of intermolecular interactions involving sulfur, oxygen, and hydrogen atoms in organic compounds.

Type of atoms present in the crystal structures	Number of structures, among the 348445 reports*
Sulfur (S)	29365
S and Hydrogen (H) together	29003
Oxygen (O)	116876
O and H together	116415
S, O, and H together	21609

Type of interactions	Number of compounds	Number of interactions	Number of compounds	Number of interactions
	Among the 29003 reports, containing S and H together		Among the 21609 reports, containing S, O, and H together	
S−H⋯O		–	25	32
S−H⋯S	18	24	8	11
S−H⋯X	80	157	44	69
X−H⋯S	11557	27227	7913	17738
	Among the 116415 reports, containing O and H together			
O−H⋯O	23065	>65000	2840	7647
O−H⋯S		–	1268	2298
O−H⋯X	28094	>65000	3517	20813
X−H⋯O	81173		15334	>65000

*CSD Version 5.26 [November 2004]+1 Update [February 2005]; Total number of reported structures: $325709 + 12736 = 348445$; terminal hydrogen positions are normalized. Intermolecular distances searched are within sum of van der Waals radii.

chemistry and biology' [28] that the S−H group, though generally classified as rather a weak donor in organic chemistry, the degree of activation of its donor ability can become substantially strong depending on the environment provided in the crystal lattice. They suggest that more often in the literature, it is found that the H-bonds formed by S−H groups are weak allowing the rotation of the thiol group, leading to disorder. This creates a problem in the location of the H-atom and indeed, a large fraction of the thiol group with unrealistic geometries is found in CSD. We have once again systematically looked at the capability of sulfur to be cooperative (act both as donor and acceptor) and have compared the corresponding interactions involving oxygen. Table 1 provides the statistical detail of the occurrence of intermolecular interactions and, in particular, brings out the dominance of the acceptor capability of the S-atom. It is noteworthy that a comparative analysis of the cooperativity involving the O-atom, which is present in a significantly larger number of interactions, shows that the S-atom, as an acceptor is strikingly favored, in agreement with an analysis performed earlier [28].

The description of the charge-density distribution in the vicinity of an S-atom appears to be difficult as can be seen from the very few charge-density studies in sulfur-containing compounds [30,47–65]. It is often seen that the multipole description of an S-atom is inadequate, mainly because of the fact that the S-atom can simultaneously display donor as well as acceptor characteristics. In our own earlier studies [30,62] the inadequacies of the multipole model to describe the features around the S-atom has been highlighted and it is imperative that more charge-density data sets on structures containing differently substituted S-atoms need to be analysed.

3. Charge densities from X-ray diffraction

In a typical molecule, the distance between the constituent atoms is of the order of 0.1 nm and hence X-rays, which possess wavelengths in the nanometre range, are most ideally suited to probe this regime, to gain inputs to see the shapes and also to visualize how molecules interact with each other in a molecular crystal. X-rays are scattered, in general, by the electrons in the atom and hence provide the means for plotting the electron density distribution in the crystal space. The term 'charge density' is more appropriate [66] to use than 'electron density' because chemically useful properties such as electrostatic potentials, molecular moments, electric field gradients along with electron distribution and its topological properties is contained in the X-ray diffraction experiment, which utilizes both positive and negative charges. As mentioned earlier, several authoritative reviews [1,7,8,66] have already appeared in the literature and our current emphasis would be to provide a brief survey to elucidate the utility of charge densities from X-ray diffraction experiments to probe weak intermolecular interactions.

3.1. *Experimental method and data analysis*

The accuracy and the quality of the data are highly dependent on the conditions and the method adopted in the experiment. In charge-density studies the data collection, processing, and refinement should be performed with enormous care, as precision in data is a prerequisite [67]. The current state of the art of data acquisition is with either conventional X-rays of fixed lower wavelength [e.g. $\lambda(MoK_\alpha) = 0.7103\,\text{Å}$] or with synchrotron X-rays (tunable for lower wavelength, typically $\sim 0.4\,\text{Å}$) as a source and with a CCD or an image plate (IP) as detector. The rate-limiting step is in the quality of the crystal itself. It is an essential requirement that one obtains measurable data covering the entire reciprocal space up to the highest possible resolution. This is made possible by the use of a combination of shorter wavelength and lower temperature measurement. A significant lowering in thermal diffuse scattering is seen in data sets collected at low temperatures (100 K and below using cryosystems with N_2 flow or using He cryostat), which will allow reflections to be measured at high scattering angles. Several reviews, in particular those of Spackman [7,8], Kortisánszky and Coppens [1], have detailed the methodology followed for collection and reduction of extremely accurate data and the experimental conditions that are used in charge density analysis.

We shall restrict ourselves to describe the experimental methodology for systems considered as examples later in this review. High-resolution X-ray diffraction data were collected on a Bruker AXS SMART APEX CCD diffractometer using MoK_α radiation operating the X-ray generator at 50 kV and 40 mA. All the data sets have been collected at 90.0(2) K using the Oxford cryo-system with N_2 flow (cooling ramp rates were generally set at 40 K/hr). Suitable crystals were grown by solvent evaporation (slow) methods and selected under an Olympus SZX12 optical microscope equipped with an optical polarizer and Olympus DP11 digital camera. The data sets were collected with crystals enclosed in a Lindemann capillary and were allowed to stabilize at the final temperature (90 K) for about an hour. The unit-cell parameters were then determined repeatedly until the estimated standard deviations in cell dimensions did not vary beyond acceptable limits. The data were collected in several steps with

Table 2.   A summary of the 90 K X-ray data collection strategy.

Run number	Starting frame number	Angle 2θ (°)	ω (°)	ϕ (°)	χ (°)	Axis	Angle width (°)	Total frame numbers	Exposure time* (Sec.)
1	001	−25	−25	0	54.79	2	0.3	606	15
2	001	−25	−25	90	54.79	2	0.3	606	15
3	001	−25	−25	180	54.79	2	0.3	606	15
4	001	−25	−25	270	54.79	2	0.3	606	15
5	001	−50	−50	0	54.79	2	0.3	606	30
6	001	−50	−50	90	54.79	2	0.3	606	30
7	001	−50	−50	180	54.79	2	0.3	606	30
8	001	−50	−50	270	54.79	2	0.3	606	30
9	001	−75	−75	0	54.79	2	0.3	606	45
10	001	−75	−75	90	54.79	2	0.3	606	45
11	001	−75	−75	180	54.79	2	0.3	606	45
12	001	−75	−75	270	54.79	2	0.3	606	45

*May vary from crystal to crystal.

different scan times (see table 2) to cover the full-sphere of reciprocal space with different 2θ settings of the detector ($-25°, -50°$, and $-75°$) and φ settings ($0°, 90°, 180°$, and $270°$) of the goniometer and the scanning angle ω was set to $0.3°$ for each 606 frames. The crystal to detector distance (optimized) was kept at 6.03 cm. This strategy (see table 2) [62] provides high resolution, large redundancy and better completeness in data sets, which are the key factors for multipole refinement modeling. The data collection was monitored using SMART [68] and reduced with the packages SAINTPLUS [68], which takes care of several systematic errors. Sorting, scaling, merging, and empirical correction for absorption of the set of intensities were performed with program SORTAV [69]. The structures were solved by direct methods using SHELXS97 [70] and refined in the spherical atom approximation (based on F^2) by using SHELXL97 [70] included in a complete package WinGX [71]. The molecular diagrams were generated using ORTEP [72].

3.2. *Multipole formalism, XD package, and multipole refinement strategy*

The nature of chemical bonding and interactions can be evaluated in terms of the deformation densities, which have been calculated based on Hansen and Coppens multipole formalism [14] as described in the earlier section. A number of least squares refinement programs have been developed, and utilized by various groups [14,15,35,73–75]. The package XD [15] is the most widely used for the analysis of experimental diffraction data. The structure of the present version of XD (Revision: 4.10, 23 July 2003) contains several components as given in figure 1. This package can be used for multipole refinement and hence the topological analysis of charge densities from the measured structure factors. XD manual (Version February 2004) describes the methodology and the applications of each module in detail. The module XDINI provides the interface between XD and the packages used for solving and refining the structures, for example SHELX. It creates the master file and the required input files for the module XDLSM, which is a full-matrix least squares program and it is based on the Hansen and Coppens formalism. It is to be noted that the major component of XDLSM is based on the program MOLLY [14] and it
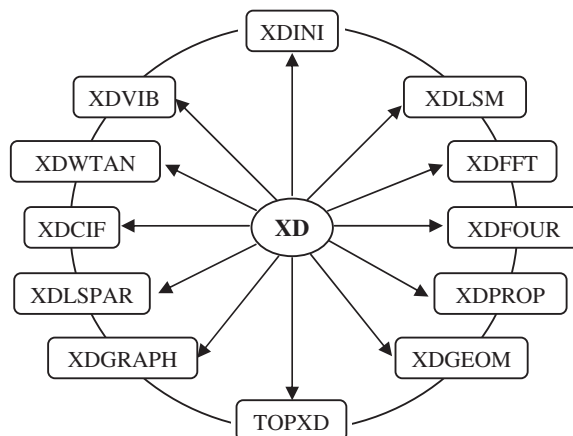
Figure 1. The structure of the present version of XD (Revision: 4.10, 23 July 2003).

allows one to locate the inadequacies in the model, to control the refinement, and to monitor the results. The strategy of multipole refinement is very crucial and it is difficult to suggest one specific scheme. However, the following strategy was found to provide a good model for organic molecular crystals [30,62,76] described later in this review. Initially only the scale factor was refined with all reflections. Next, to determine the accurate positional and thermal parameters the higher order ($\sin\theta/\lambda \geq 0.8\,\text{Å}^{-1}$) refinements were performed for non-H-atoms. The positional and isotropic thermal parameters of the H-atoms were then refined using the lower angle data ($\sin\theta/\lambda \leq 0.8\,\text{Å}^{-1}$). Due to unavailability of the neutron data, the positions of the H-atoms in this refinement as well as in the subsequent refinements were fixed at the average bond distance value obtained from reported neutron diffraction studies [77]. In the next stage of refinements releasing monopole, dipole, quadrupole, octapole, and hexadecapole (if required) populations with single κ were performed in a stepwise manner. Finally a single κ' was refined for each species for all non-H-atoms along with the rest of the parameters (including the isotropic thermal parameters of H-atoms). For all H-atoms the multipole expansion was truncated at $l_{\max}=1$ (dipole, bond-directed) level. For chemically different groups of non-hydrogen atoms, separate κ and κ' were allowed while for H-atoms the corresponding values were fixed at 1.2. No space group symmetry or chemical restraints were applied, but the molecular electroneutrality constraint was applied and the scale factor was allowed to refine throughout all refinements. The real and imaginary dispersion corrections to the form factors [78] were used in all the structure factor calculations. Scattering factors were derived from the Clementi and Roetti [79] wave functions for all atoms. The function minimized in the least-squares refinement is $\sum w\left(|F_0|^2 - K|F_c|^2\right)^2$ for all reflections with $I > 3\sigma(\boldsymbol{I})$. The residual bonding density, not modeled in the conventional spherical refinement, is taken into account in this multipolar refinement. The module XDFFT is a 3-dimensional fast Fourier transform program, which allows the determining of the extrema of the residuals or the dynamic deformation density over the whole unit cell after the refinement. This program is much faster than XDFOUR, which also measures the residual and the dynamic deformation density

over a given range. The static electron density, which has been obtained in the form of a nuclear-centered multpole expansion, can be analysed via XDPROP. This program can be used to evaluate the one-electron properties such as net charges, electrostatic potentials, dipole moments etc. and to carry out the CP analysis of the total electron density. The program XDGEOM calculates the various functions of the atomic coordinates together with the standard uncertainties and the symmetry related atoms in the lattice. Additionally, it creates a crystallographic information file (CIF) and multipole population parameter file. The quantum theory of AIM is fully incorporated in the module TOPXD [80], which provides an extensive set of atomic properties, including Bader charges, dipole, and higher electrostatic moments along with atomic volume and atomic nuclear-electron potential energy by integration over atomic basins. The specific results from the programs mentioned above can be visualized via an independent graphical package XDGRAPH, which allows for 2-dimensional (contour or height field), 3-dimensional (isosurface), molecule, bond path, and relief plots. The code XDLSPAR can be used to get the values of the parameters used in the multipole refinements and the corresponding outcomes of the refinement. Additionally, there are a few XD utility programs such as XDCIF (to create an archive CIF), XDWTAN (to analyse the weighting scheme), and XDVIB [to calculate the mean square displacement amplitude (MSDA) from harmonic vibrational frequencies and normal modes]. A new module recently interfaced to the XD package is XDINTER [2,81], which utilizes the experimental charge density approach (ECDA) and allows the evaluation of the intermolecular interaction energies and hence the lattice energy. The calculation based on Spackman's set of the exp-6 atom–atom potentials [82] results in the evaluation of the binding energy in terms of the electrostatic, exchange-repulsion, and dispersion components. The corresponding lattice energies are estimated by subtracting the relaxation energies (obtained from GAUSSIAN98 described later) from the value of the binding energies [2,83].

3.3. *Topological analysis, atoms in molecule approach*

The surface features, or topology, of the charge-density distribution obtained from experimental or theoretical methods can be analysed via Bader's quantum theory of AIM approach [18,19]. This approach provides a pathway for comparing the experimental electron density with the theoretically derived density in terms of topological properties of the charge density $\rho(\mathbf{r})$. The topology of the scalar field, such as $\rho(\mathbf{r})$, which is a physical quantity, can conveniently be summarized in terms of CPs, where the first derivatives of $\rho(\mathbf{r})$ vanishes, $\Delta\rho(\mathbf{r}) = 0$, indicating the position of extrema (maxima, minima, or saddles) in the $\rho(\mathbf{r})$ at $\mathbf{r}_c$. In general, the theory of AIM provides a methodology for the identification of a bond between any two atoms in a molecule in terms of CP, called bond critical points (BCP). This analysis is based on the identification of CP, classified using the Hessian matrix of the electron density [18,21] which is a 3×3 ordered array of the second derivatives of $\rho(\mathbf{r})$. The Hessian matrix generates three eigenvectors, which are mutually orthogonal and coincide with the so-called *principal axis of curvature*. This suggests that each eigenvector represents an axis and the corresponding eigenvalues (λ_1, λ_2, and λ_3 with $\lambda_1 \leq \lambda_2 \leq \lambda_3$) determines the profile of the electron density along this axis. The number of non-zero curvatures of the Hessian matrix defines the *rank* associated with the CP and the *signature* of a CP is the sum of the signs of the curvatures and in general, a CP is labeled by giving both

its rank and signature. It is noteworthy that the CPs in a stable molecule are all of rank 3, which gives rise to four possible type of CPs:

(3, −3) Peaks: all curvatures are negative and ρ is a local maximum at $\mathbf{r}_c$.

(3, −1) Passes or saddle points: two negative and one positive curvatures; $\rho(\mathbf{r}_c)$ is a local maximum along two of the axes and a local minimum along the third orthogonal axis, found between every pair of nuclei linked by a chemical bond.

(3, +1) Pales: two positive and one negative curvatures; $\rho(\mathbf{r}_c)$ is a local minimum along two of the axes and a local maximum along the third orthogonal axis, found at the center of a ring of bonded atoms.

(3, +3) Pits: all three curvatures are positive and ρ is a local minimum at $\mathbf{r}_c$.

For intermolecular interactions, the CPs of the type (3, −1), and the properties of $\rho(\mathbf{r})$ at these points, which provide the chemically most useful information, are of great interest. The line of the highest electron density linking any two atoms is referred to as the *bond path* and its length R_{ij} (need not be the same as inter-atomic vector) is referred to as the *interaction line*, which passes through the BCP. The existence of a (3, −1) CP and associated BP is the topological definition of a chemical bond. For a strained system the BPs deviate from the inter-nuclear vectors. If the charge is preferentially accumulated in a particular plane along the BP, the bond will no longer be cylindrical, rather it will have an elliptical cross section ($\lambda_1 \neq \lambda_2$). A quantitative measure of the ellipticity of a bond, *bond ellipticity* is defined as $\varepsilon = \lambda_1/\lambda_2 - 1$, where λ_2 is the curvature of smaller magnitude. The strength of a bond or the *bond order* is defined by the magnitude of the charge density at the BCP, ρ_b. An important function of $\rho(\mathbf{r})$ is its second derivative, the *Laplacian* $\nabla^2\rho(\mathbf{r})$, is a scalar quantity and defined as the sum of the principal curvatures ($\lambda_1 + \lambda_2 + \lambda_3$), it is a representation of the chemical features of the molecule. The physical significance of the Laplacian is that it represents areas of local charge concentration and depletion. If $\nabla^2\rho_b(\mathbf{r}) < 0$, the density is locally concentrated resulting in shared interactions, while in the case of $\nabla^2\rho_b(\mathbf{r}) > 0$ the electron density is depleted representing closed-shell interactions. It is possible to observe lone pairs in the Laplacian as these appear as local maxima, i.e. (3, −3) CPs in the negative Laplacian. The electron density, Laplacian, interaction line, the curvatures, and the bond ellipticity together represent the topology of the charge density distribution in a given molecule. Thus the AIM approach could be used for both theoretical and experimental analysis.

3.4. *Molecular crystals, one-electron properties*

Molecular crystals offer the advantage of getting substantial information on properties, which mainly depend on the charge-density distribution. For example, one-electron properties like net charges, dipole moments, electrostatic potential, polarizabilities, and hyperpolarizabilities could be evaluated quantitatively in such crystals. The XD package as described in the previous section provides routines XDPROP and TOPXD, which can be employed to obtain the values for one-electron properties. Charges obtained from AIM analysis based on integration over atomic basins can be directly compared with those obtained from experimental charge-density studies. Electrostatic potential surfaces provide information on the nature and topology of the distribution of charges, which offer inputs for the calculation of intermolecular

interaction energies and crystal dipole moments. Using the ECDA it is possible to obtain the intermolecular interaction energy (E_{int}) from the multipole description [80,83] using the package XDINTER. A comprehensive discussion on molecular dipole and quadruple moments has been published in 1992 including a list of dipole moments estimated from experimental charge-density studies as compared to *ab initio* theoretical results on a large number of molecular crystals [66]. During recent years it has been recognized that the solid-state molecular dipole moment obtained from reliable theoretical calculations tends to be significantly smaller than those derived from the multipole analysis of diffraction data [62,84,85]. The larger the polarity of the molecule in the crystal, the differences become more substantial, and it has been suggested that periodicity plays a significant role in the enhancement of the value of the dipole moment in the crystal. A significantly large number of experimental charge-density studies have been focused on the elucidation of nonlinear optical (NLO) properties of molecular crystals [86–88]. The major concern originates from the fact that compounds exhibiting second harmonic generation (SHG) effects, crystallize in non-centrosymmetric space groups (a prerequisite) and the dipole moment values strongly depend on the nature of the packing of the molecules, while there is always a concern about the ambiguity in phase determination. However, the enhancement observed in the molecular dipole moment values does not seem to originate from errors in phase determination, instead it is more due to alignments of molecules along the polar axis [1].

4. Charge densities from theory

Theoretical methods, in particular those which provide computational pathways depending on no experimental values other than fundamental constants are said to be *ab initio*. It is remarkable that these computational methods on high-speed computers allow for the evaluation of several chemical or physical properties of a system, including proteins. A practical level of theory assumes the Born–Oppenheimer approximation, thus providing an effective separation between electronic and nuclear motion. The wavefunction for describing a one-electron system incorporates the Pauli exclusion principle and the resulting differential equation is referred to as an HF equation. In general, this equation is solved *via* an iterative process and the convergence is achieved once a self-consistent field (SCF) is obtained. The use of molecular orbitals (MO) to describe a molecule containing n electrons involves the linear combinations of atomic orbitals (LCAO) approach. This requires the choice of basis functions, which in modern quantum chemistry are referred to as 6–31 G*, STO-3 G etc. The most typical route to solve the Schrödinger equation is to have an HF–SCF–MO–LCAO approach. The HF scheme successfully predicts the properties of a system near the ground-state equilibrium geometry, however, ignoring the correlation energy. The methodology involved in density functional theory (DFT) includes electron correlation and hence is the desired method for obtaining theoretical charge density in molecular crystals. DFT, over the years has become a practical tool for calculating charge-density distributions since its adaptability to high-speed computers is easy. The level chosen for electron density in the DFT method is generally B3LYP [88,89] and the corresponding Gaussian basis set is 6-31G** [90], which takes into account polarization and diffuse functions. The presence of symmetry elements in molecular crystals has a significant

role to play and the computational package CRYSTAL03 has been developed to incorporate the periodicity in molecular crystals.

4.1. *Periodic calculations, CRYSTAL03 package*

The package CRYSTAL03 [17] is an *ab initio* program, which performs the calculation within the LCAO approximation to estimate the ground-state energy, energy gradient, electronic wavefunctions, and properties of periodic systems. These periodic systems can be molecules (0-dimension), polymers (1-D), slabs (2-D), and crystals (3-D). This program expects the geometry and symmetry information of the crystal lattice and the basis set for each atom as inputs. The choice of the basis set is crucial because of the many possible variations in chemical bonding of a periodic system, for example a carbon atom in diamond has a different bonding environment compared to a carbon atom in a phenyl ring in the crystal lattice. Choosing a basis set is of paramount importance and very often conflicting issues arise in terms of accuracy and computational cost, accuracy being the main goal in *ab initio* calculations. Use of a large but well-defined basis set with complete flexibility involves a large number of variational parameters and hence the resulting wavefunction is very close to the actual wavefunction of the system. An associated major problem is the basis set superposition error (BSSE), superposition of the basis functions of the two subsystems [92], which can be estimated by means of the counterpoise method [93] with the consideration of the 'ghost functions'. The BSSE corrected wavefunction can be used to derive accurate one-electron properties and the X-ray structure factors (static) of the crystal. The examples reported later in this review are based on the experimental geometry and the method used is DFT at B3LYP level with 6-31G** basis set. This basis set has been shown to provide reliable and consistent results with respect to studies involving intermolecular interactions [30,76,94]. The general procedure and conditions to obtain static structure factors are described in the following. In *ab initio* calculations for periodic structures, the integration in reciprocal space is an important aspect and in practice, the corresponding shrinking factors (IS1, IS2, and IS3) along the reciprocal lattice vectors can be set at 4 (30 K-points in the irreducible Brillouin zone). The truncation parameters (ITOL), which control the accuracy of the calculation of the bielectronic Coulomb and exchange series, can be set at $ITOL1 = ITOL2 = ITOL3 = ITOL4 = 8$ (half of ITOL5). Due to the large difference between ITOL4 and ITOL5 the exponents of the polarization functions need not be scaled [92]. The eigenvalue level shifting technique is well known in molecular studies [95,96] and has been extended to the periodic systems. It accelerates the convergence during the calculation and a rapid convergence in energy can be achieved by setting the level shifter value at 0.3 or 0.5 Hartree. Upon convergence with respect to the energy value $\sim 10^{-6}$, the obtained periodic wavefunctions are used to generate the theoretical structure factors with the option XFAC. These static structure factors are free from several factors, in particular those related to thermal and zero point motion of nuclei.

To eliminate an important source of correlation between parameters, the temperature factors and atomic positions are held fixed during the multipole refinement of the theoretical structure factors *via* XD. After a scale factor refinement, the same multipoles, as used in the refinement of experimental structure factors, are allowed to refine with separate κ' parameters for each non-H-atom including all theoretical reflections.

The modules XDPROP and TOPXD implemented in the package XD are used for topological analysis of the theoretical electron density.

The lattice energies were calculated based on the procedure [83] described by Abramov *et al.*, which defines the lattice energy as the difference between the molecular interaction energy in the crystal and the molecular relaxation energy upon sublimation. The molecular interaction energy was evaluated as the difference between the energy of the molecule in the crystal to that of the isolated molecule with the crystal geometry. CRYSTAL03 was used to obtain the molecular interaction energy after correcting for BSSE. Relaxation energy was obtained as the difference between the energy of the isolated molecule with optimized geometry and the molecule with crystal geometry. GAUSSIAN98 was used to obtain the relaxation energy at the HF and B3LYP level with 6-31G** basis set.

4.2. *Atomic basin properties*

The gradient paths originate at infinity and terminate at the nucleus after traversing a section of space known as the 'atomic basin'. Aicken and Popelier [97] have described the details of atomic integration and the evaluation of atomic charges, electrostatic moments, volumes, and energies along with other atomic properties. The module TOPXD implemented in the package XD allows for the calculation of these properties in the crystal while the program MORPHY98 [98] provides the corresponding information in the gas-phase for the isolated molecule. *Ab initio* geometry optimization and the corresponding wave functions for the isolated molecule are obtained *via* GAUSSIAN98 from different methods at various levels with a proper basis set. In the calculations performed to evaluate the atomic basin properties, both in the crystal and in the gas-phase, similar values should be used for the integration variables. The HF level calculations have produced reliable atomic basin properties in several examples [20,98,99]. However, we have used the B3LYP/6–31G** level to calculate these properties to enable a direct comparison of the results between an isolated molecule and a theoretical crystal [30,76].

4.3. *Koch and Popelier's criteria*

The topological analysis, however, does not specify the character of the bond but only indicates the existence of a bond. In order to characterize a bond in terms of its chemical concepts such as bond order, ionicity, conjugation, and hydrogen bonding the properties evaluated at the BCPs become crucial. Koch and Popelier have proposed eight criteria to establish hydrogen bonding in particular, which distinguish a hydrogen bond from a van der Waals interaction [20,21]. If one or more of these criteria are not satisfied, the interaction concerned can be considered as a van der Waals interaction. Among these eight criteria, the fourth condition is considered as *necessary and sufficient* to describe fully a hydrogen bond. The **first** condition is the presence of a BCP between a donor atom and an acceptor atom linked *via* a BP. The **second** condition is the presence of charge density evaluated at the BCP and its relationship with the overall hydrogen bond energy. It is possible to relate the charge density parameters at the BCP to the local energy density $E(r_{CP})$ of the electrons by evaluating the local electronic kinetic energy density $G(r_{CP})$ and the local potential energy density $V(r_{CP})$ using the

equations [18,100,101],

$$G(r_{CP}) = \left(\frac{3}{10}\right)(3\pi^2)^{2/3}\rho^{5/3}(r_{CP}) + \left(\frac{1}{6}\right)\nabla^2\rho(r_{CP}),$$

$$V(r_{CP}) = \left(\frac{1}{4}\right)\nabla^2\rho(r_{CP}) - 2G(r_{CP}), \quad \text{and}$$
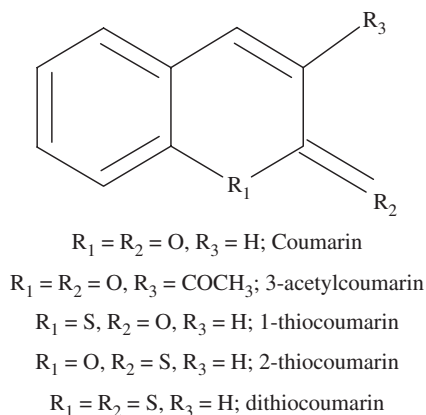
$$E(r_{CP}) = G(r_{CP}) + V(r_{CP})$$

The **third** condition refers to the value of the Laplacian at the BCP. The calculated values of $\nabla^2\rho_b(\mathbf{r})$ should be positive and should correlate with the interaction energy. The value of $\nabla^2\rho_b(\mathbf{r})$ should also agree with the range of values found so far in the literature. The **fourth** condition deals with the mutual penetration of the hydrogen and the acceptor atom. This condition, considered as **necessary and sufficient**, compares the non-bonded radii of the donor-hydrogen atom (r_D^0) and the acceptor atom (r_A^0) with their corresponding bonding radii. The non-bonding radius is taken to be equivalent to the gas phase van der Waals radius of the participating atoms [102,103]. The bonding radius (r) is the distance from the nucleus to the BCP. In a typical hydrogen bond, the value of $\Delta r_D = (r_D^0 - r_D) > \Delta r_A = (r_A^0 - r_A)$ and $\Delta r_D + \Delta r_A > 0$ represent positive interpenetration. If either or both of these conditions are violated, the interaction is essentially van der Waals in nature.

The rest of the four criteria are obtained from integration over the atomic basins of the participating H-atoms. The **fifth** condition states that the H-atom loses electrons resulting in an increased net charge on the H-atom. The **sixth** condition concerns the energetic destabilization of the H-atom strongly correlating with the fifth one. The difference in total energy between the crystal and the bare molecule should be positive. The **seventh** condition suggests a decrease of dipolar polarization (magnitude of the first moment, M) of the H-atom upon hydrogen bond formation. H-atomic volume depletion forms the basis for the **eighth** condition.

5. Examples

5.1. *Coumarin and its derivatives*

Coumarin has been extensively studied as it finds applications in several areas of synthetic chemistry, medicinal chemistry, and photochemistry. The formation of a [2 + 2] cyclo-addition product upon irradiation [104] of coumarin and its derivatives has contributed immensely to the area of solid-state photochemistry. Several substituted coumarin derivatives find application in the dye industry [105,106] and in the area of LASER dyes [107,108], based on the property of these compounds showing state-dependent variation in the static dipole moment. Coumarin dyes such as coumarin 138 [109], coumarin 152 [110], coumarin 153 [111] and coumarin 314 [112] exhibit polymorphism. Further, 4-styrylcoumarin [113], a fluoro derivative of coumarin [114], and 3-acetylcoumarin [115] also display polymorphism [116]. A wide variety of pharmacological activities, such as antiviral [117] and antimicrobial activity [118] are exhibited by coumarin derivatives and form the basic building block in the well-known antibiotic Novobiocin [119]. Coumarin and its sulfur derivatives possess

$R_1 = R_2 = O$, $R_3 = H$; Coumarin

$R_1 = R_2 = O$, $R_3 = COCH_3$; 3-acetylcoumarin

$R_1 = S$, $R_2 = O$, $R_3 = H$; 1-thiocoumarin

$R_1 = O$, $R_2 = S$, $R_3 = H$; 2-thiocoumarin

$R_1 = R_2 = S$, $R_3 = H$; dithiocoumarin

Scheme 1.   The molecular diagram of coumarin and its derivatives.

well-defined dipole moments and exhibit SHG effects since they crystallize in noncentrosymmetric space groups [120,121]. We have studied the geometry and the molecular packing patterns of several coumarins and their derivatives [104] in order to evaluate the features of noncovalent interactions. In this context, we have been interested in coumarin (**1**), 3-acetylcoumarin (polymorphic forms) (**2**), 1-thiocoumarin (**3**), 2-thiocoumarin (**4**), and di-thiocoumarin (**5**) (Scheme **I**) particularly to understand and characterize weak intermolecular interactions such as $C-H \cdots O$, $C-H \cdots C_\pi$, $C_\pi \cdots C_\pi$, $C-H \cdots S$, and $S \cdots S$. It is of importance to note that in all these structures the dominant interactions are all weak and there are no highly directed strong hydrogen bonds. This unique feature has been exploited, as can be seen from the following examples, to characterize quantitatively the features associated with the crystal engineering tools offered mainly by weak intermolecular interactions.

5.2. *Experimental and theoretical charge density distribution, topological features*

5.2.1. Coumarin (2H-chromene-2-one) [30].   This is a simple planar organic molecule, crystallizing in a non-centrosymmetric space group, $Pc2_1b$, exhibiting SHG effects (see table 3) and hence is an ideal choice for charge-density analysis. Figure 2 gives the molecular ORTEP with 50% probability for non-H-atoms from the data collected at 90 K, showing the atom labeling. Hirshfeld's rigid bond test [122] was applied during the final refinement for intra-molecular bonds, not involving H-atoms. The maximum difference of MSDA (DMSDA) value is found to be $6 \times 10^{-4} \text{Å}^2$ for the bonds C(4)–C(5), indicating that the atomic thermal vibrations have been accounted for properly. The minimum and the maximum residual densities over the entire asymmetric unit are in the range of -0.241 to $+0.174 \, \text{eÅ}^{-3}$ depicting the correctness of the model. The corresponding dynamic deformation density map (not shown here) indicates the accuracy in the chemical bonding features of the molecule. The static maps (devoid of thermal smearing) obtained from multipole analysis of both experimental and theoretical structure factors are in good agreement as can be seen from figure 3. The lone pair of electrons on the O-atoms is prominently seen in both cases. The electron density and Laplacian values at the BCPs are found to be in good agreement,

Table 3. Molecular dipole moments of coumarin and its derivatives and their SHG activity.

| | Molecular dipole moments (Debye) | | | |
| | Crystal | | | |
Compound	Experiment	Theory (B3LYP/631G**)	Single molecule (optimized) (B3LYP/631G**)	SHG activity* (Compared with Urea)
Coumarin	13.5 (12)	8.1	4.8	1.051
3-Acetylcoumarin (Form **A**)	18.0(2)	13.5	7.5	–
3-Acetylcoumarin (Form **B**)	9.7(6)	3.6	4.3	–
1-Thiocoumarin	19.2(19)	10.0	4.8	1.102
2-Thiocoumarin	17.4(9)	12.0	5.8	0.989
Dithiocoumarin	14.1(11)	12.5	5.8	0.949

SHG activity measurement details:
Laser used: Quanta Ray DCR3 LASER.
Wavelength and frequency: 1064 nm, 20 Hz.
Power = 10 mJ/pulse = 11.11 GW.
FWHM = 70 ns.
Pulse length = 9 ns, rate = 10/s.
Rise time = 40 ns.
Scale of detection = 50 mV & 200 ns.
Note: A Photo diode was used as detector; 1064 nm was cut off by a $CuSO_4$ solution and BG38 filter.
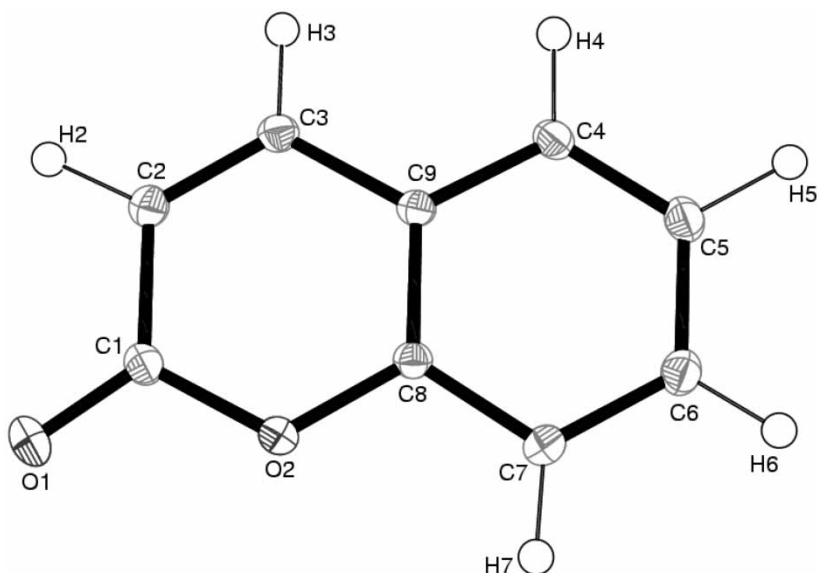
Figure 2. ORTEP view with labels for atoms of coumarin at 90 K with 50% ellipsoid probability (non-H-atoms).

demonstrating that both experimental and theoretical methodologies provide comparative measures of topological properties of charge-density distribution. The molecules pack in the crystal lattice *via* weak intermolecular interactions, four $C-H\cdots O$ hydrogen bonds and nine $C-H\cdots\pi$ interactions, identified based on the first four of the KP criteria. Figure 4 traces the bond paths (experimental) for all the $C-H\cdots O$ interactions with the $(3, -1)$ BCPs along with a representative bond path
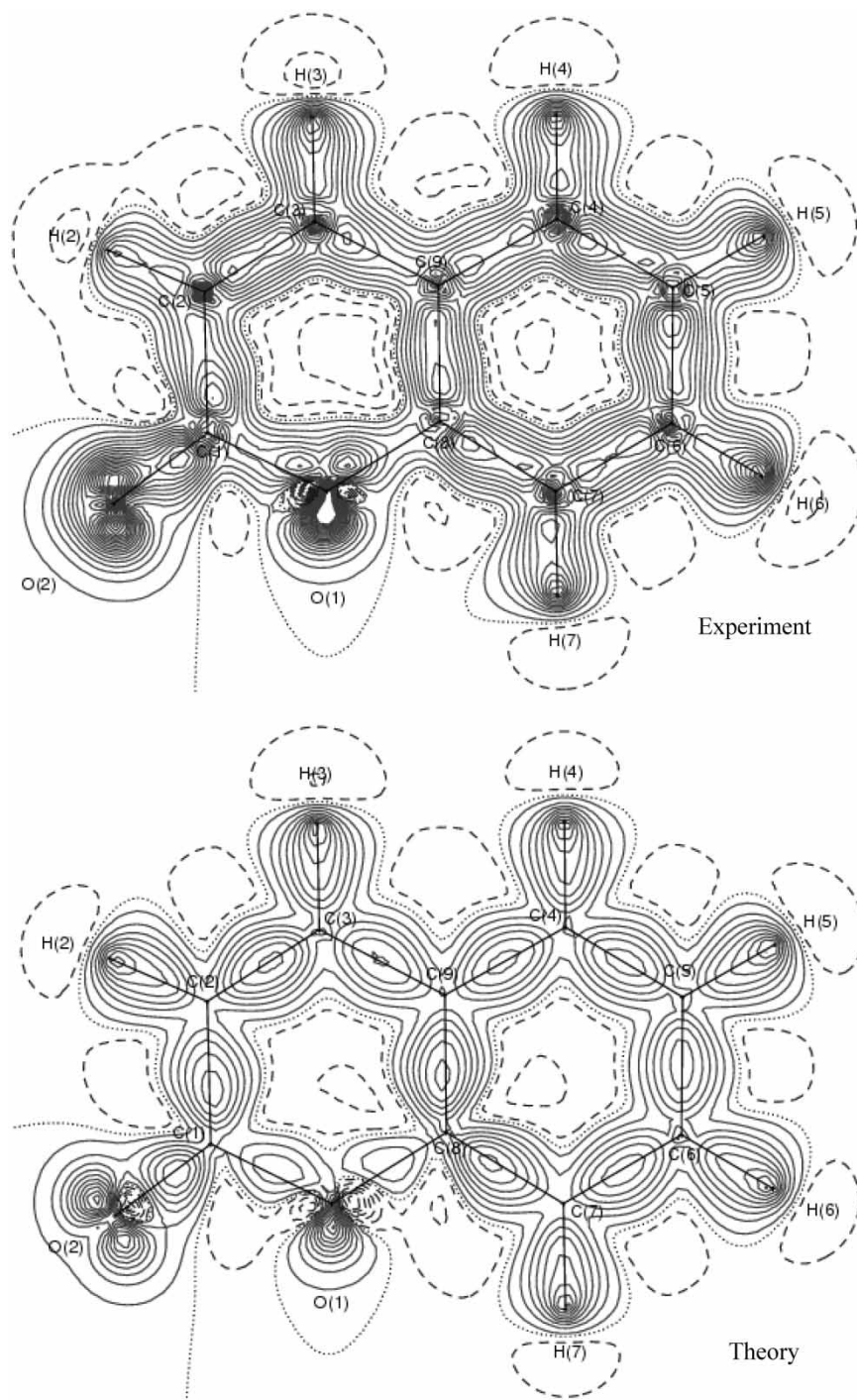
Figure 3. Static deformation density maps (experimental and theoretical) for coumarin. For all static deformation density maps, the positive (solid lines) and negative (broken lines) contour starts at $\pm 0.05 \, e\text{Å}^{-3}$ and with the intervals of $\pm 0.1 \, e\text{Å}^{-3}$, contour at zero is shown as dotted line.
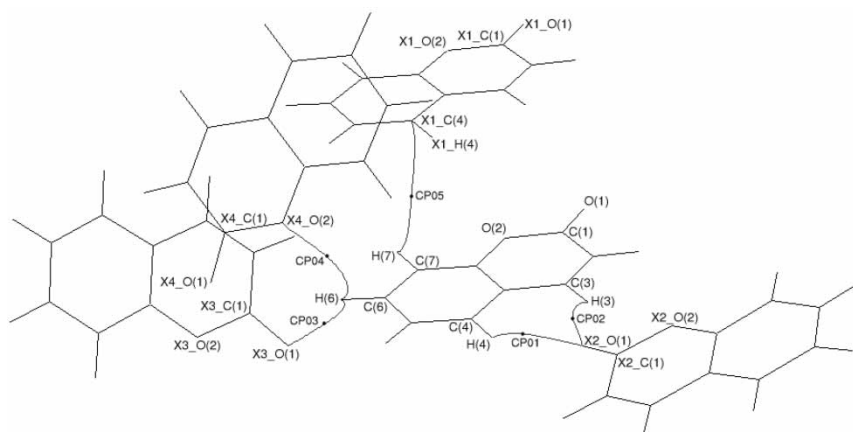
Figure 4. Bond path character in coumarin showing the critical point locations along the $C-H \cdots O$ and $C-H \cdots C_\pi$ interactions shown as dark dots.

between $C-H$ and the C_π in the molecule. Representative Laplacian maps (see figure 5) from experimental analysis, showing the distribution in the region of the BPs for these interactions and the corresponding theoretical maps (not shown here), display similar features. A significant enhancement of experimental and theoretical molecular dipole moments in the crystal was observed as compared to the single molecule optimized geometry calculation (see table 3).

5.2.2. 3-Acetylcoumarin (3-acetyl-2H-1-benzopyran-2-one) [30,76,115]. The compound exhibits concomitant polymorphism [116,123,124] (crystallizes simultaneously from the same solvent and in the same crystallizing flask under identical crystal growth conditions) and exist in two polymorphic forms, prismatic form (form **A**) and needle form (form **B**). The molecular ORTEP for non H-atoms in both forms, showing the atom labeling (see figure 6) for two molecules in the asymmetric unit in form **A** [$Z' = 2$, molecule 1 and molecule 2] and only one molecule in form **B**. Both the forms crystallized in centrosymmetric space group, form **A** in $P\bar{1}$ and form **B** in $P2_1/n$. In both forms the covalent bonds are found to satisfy Hirshfeld's rigid bond test. The minimum and the maximum residual densities over the entire asymmetric unit are -0.198, $0.219\,e\text{Å}^{-3}$ in form **A** and -0.223, $0.246\,e\text{Å}^{-3}$ in form **B**. The topological features at the intra-molecular bonding region from experiment agree well with theoretical results. The derived net charges using both experimental and theoretical structure factors, and also the charges evaluated *via* integration over the atomic basins, show significant differences with respect to the polymorphic forms. The experimental molecular dipole moments differ significantly for the two forms and the corresponding theoretical values, though lower in magnitude, show similar trends (see table 3). The lattice energies (see table 4), evaluated by the HF and DFT (B3LYP) methods with 6-31G** basis set for the two forms, clearly suggest that form **A** ($-86.1\,\text{kJ/mol}$ per monomer) is the thermodynamically stable form as compared to form **B** ($-78.7\,\text{kJ/mol}$). Mapping of electrostatic potential (see figure 7) over the molecular surface, showing dominant

(a)

(b)
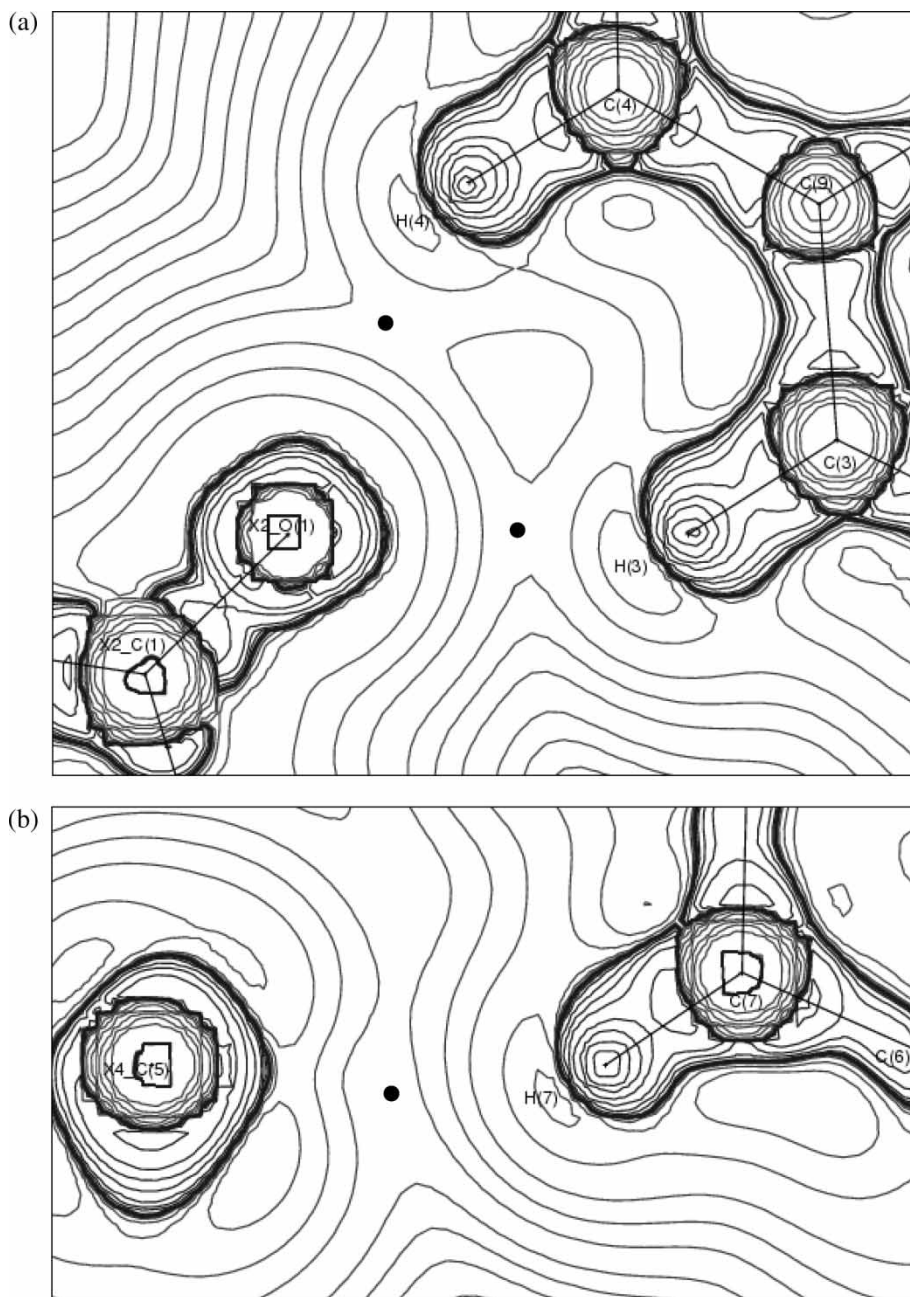
Figure 5. (a) Laplacian $[\nabla^2 \rho_b(\mathbf{r})]$ of a representative C−H⋯O intermolecular interaction in coumarin. For all the Laplacian maps the contours are drawn at logarithmic intervals in $-\nabla^2 \rho_b$ eÅ^{-5}. Dark and light lines represent positive and negative contours respectively; (b) Laplacian $[\nabla^2 \rho_b(\mathbf{r})]$ of a representative C−H⋯C$_\pi$ intermolecular interaction in coumarin.
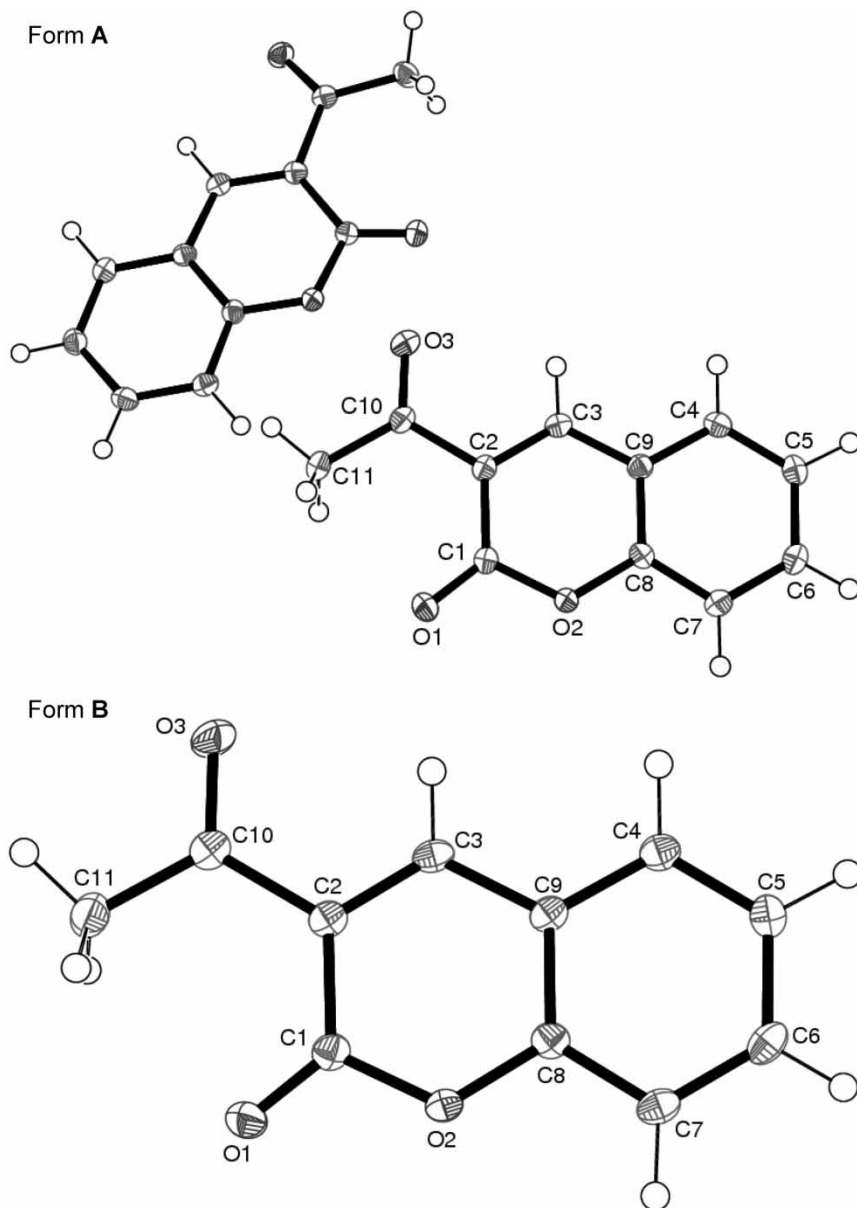
Figure 6. ORTEP view with labels for atoms of 3-acetylcoumarin at 90 K with 50% ellipsoid probability (non-H-atoms).

variations in the electronegative region, brings out the differences between the two forms. The packing features, essentially weak intermolecular interactions, of the constituent molecules mainly bring out the difference between the two polymorphic forms. Based on the first four of the KP criteria, form **A** generates eight $C-H\cdots O$ hydrogen bonds (see figure 8), nine $C-H\cdots C_\pi$, nine $C_\pi\cdots C_\pi$ (see figure 9,

Table 4. Binding energies, molecular relaxation energies, and lattice energies (kJ/mol) for form **A** and form **B** of 3-acetylcoumarin.

		Binding energies $[E_{int}]$ (kJ/mol)		
	XDINTER experimental		CRYSTAL03 HF/6-31G**	CRYSTAL03 B3LYP/6-31G**
Crystal	URMM	KRMM		
Form **A**	−299.2	−224.2	−11.0	−46.1
Form **B**	−110.2	−90.3	−3.5	−18.7

	Molecular relaxation rnergies $[E_{relaxation}]$ (kJ/mol)	
Molecule	GAUSSIAN98 HF/6-31G**	GAUSSIAN98 B3LYP/6-31G**
Form **A**	−74.5	−52.0
Form **B**	−18.8	−11.6

	Lattice energies $[E_{int} - E_{relaxation}]$ (kJ/mol)					
	Experimental (XDINTER)					
	URMM		KRMM			
Crystal	HF	DFT	HF	DFT	HF/6-31G** (CRYSTAL03)	B3LYP/6-31G** (CRYSTAL03)
Form **A**	−224.6	−247.2	−149.7	−172.2	63.5	5.9
Form **B**	−91.4	−98.6	−71.5	−78.7	15.3	−7.1

showing 7 of them), and five $C=O\cdots C_\pi$ (see figure 10) interactions, in all 31 weak interactions. The $C-H\cdots\pi$ interactions considered for this study are limited to the aromatic carbon atom region of the compound. On the other hand, form **B** generates only three $C-H\cdots O$ hydrogen bonds (see figure 8), two $C_\pi\cdots C_\pi$ (see figure 9) and two $C=O\cdots C_\pi$ (see figure 10) intermolecular interactions with no $C-H\cdots C_\pi$ interaction, in all 7 weak interactions. It is to be noted that intermolecular interactions involving H-atoms of the –CH$_3$ group are not included.

5.2.3. 1-Thiocoumarin (2H-thiochromene-2-one) [30,121]. The molecule containing an S-atom crystallizes in a non-centrosymmetric space group, *Pc*, an excellent candidate for SHG effects, showing high NLO activity (see table 3). The molecular atom labeling is shown as ORTEP with 50% probability for non-H-atoms (see figure 11). The maximum DMSDA (8×10^{-4} Å^2) is found at S(1)−C(1) bond and the minimum and maximum residual densities (−0.103 and 0.274 eÅ^{-3}), plotted over a given range (see figure 12), show the accumulation near the S-atom. The lone-pair of electrons of the S-atom is very prominent, as can be seen from the experimental and theoretical static deformation density maps (see figure 13). These features indicate the accuracy of the multipole model even with the presence of an S-atom in the molecule. The nature of packing of the molecules in the crystal lattice is governed *via* three $C-H\cdots O$ hydrogen bonds, three $C-H\cdots C_\pi$, and two $C-H\cdots S$ interactions, which were selected based on the first four of the KP criteria. All the $C-H\cdots O$ and $C-H\cdots S$ interactions, along with a representative $C-H\cdots C_\pi$ interaction, are shown in terms of BCPs and BPs in figure 14 (experimental). The $C-H\cdots S$

(a)

(b)
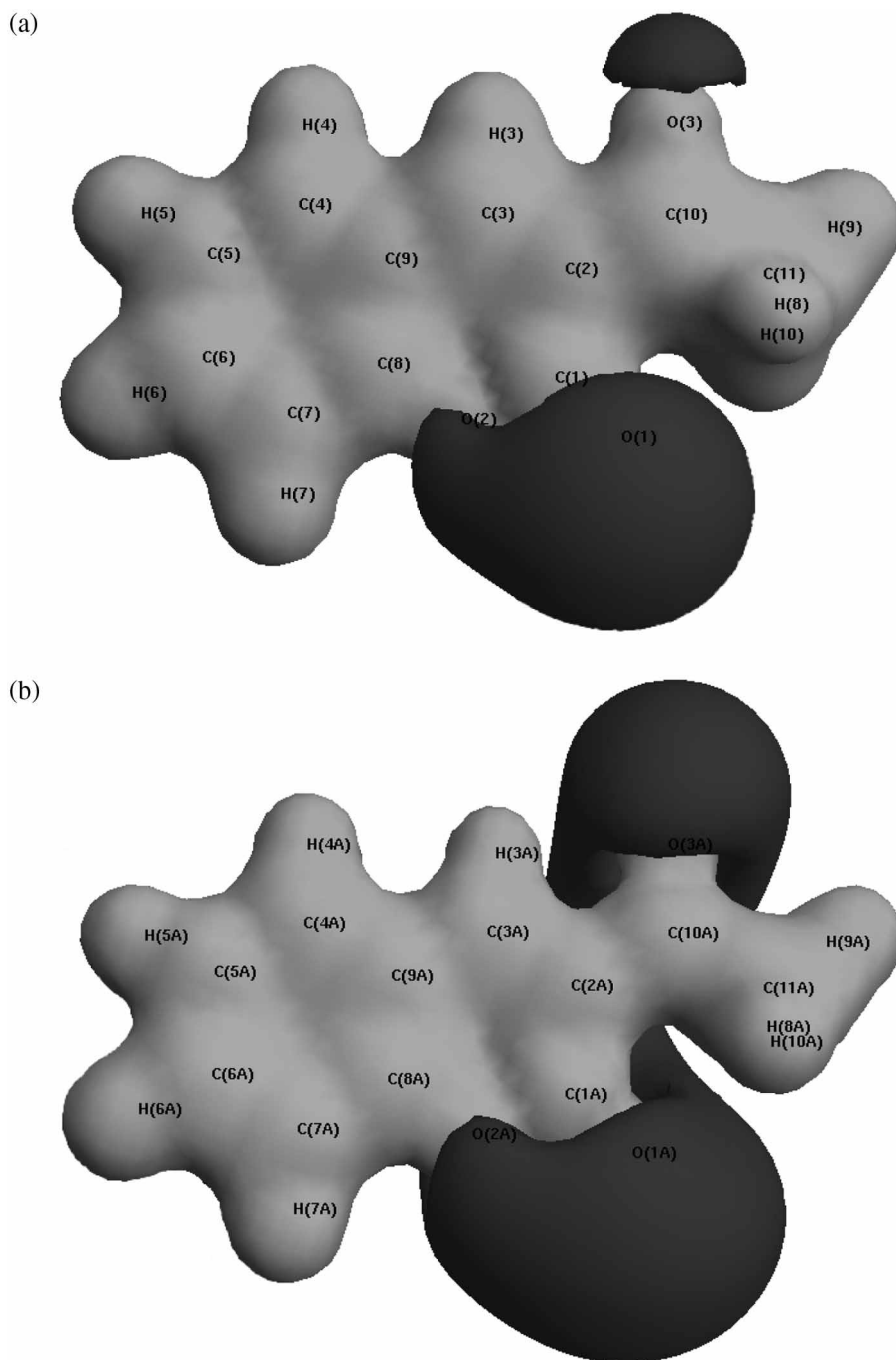
Figure 7. (a) Molecular electrostatic potential in molecule 1 (form **A**) of 3-acetylcoumarin. The potential of $+0.30\,e\text{Å}^{-1}$ is shown as the light grey isosurface while $-0.15\,e\text{Å}^{-1}$ is shown as the black isosurface in all the maps; (b) Molecular electrostatic potential in molecule 2 (form **A**) of 3-acetylcoumarin; (c) Molecular electrostatic potential in form **B** of 3-acetylcoumarin.

(c)
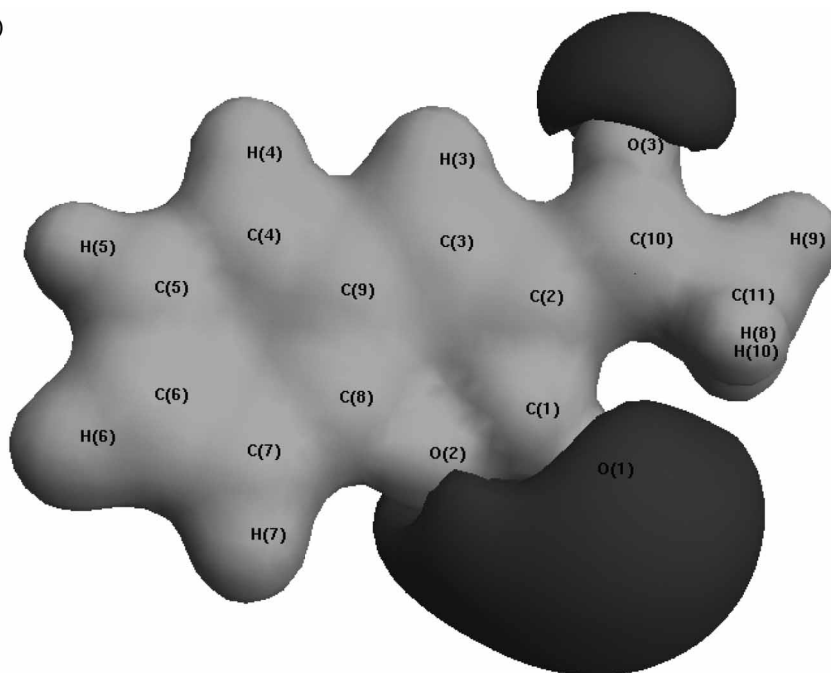
Figure 7.   Continued.

interactions are generated *via* bifurcation at the S-atom, while $C-H \cdots O$ hydrogen bonds are trifurcated at the O-atom. The $C-H \cdots \pi$ interactions considered for this study are limited to the aromatic carbon atom regions of the compounds. An enhancement of dipole moment was observed in the crystal (experiment and theory) with respect to the value obtained from single molecule geometry optimization (see table 3).

5.2.4. 2-Thiocoumarin (2H-chromene-2-thione) [62,120]**.** This sulfur derivative of coumarin crystallizes in non-centrosymmetric space group, $P2_12_12_1$ with high NLO activity (see table 3), which can be used as SHG material. Figure 15 shows the ORTEP view together with the numbering of the atoms for non-H-atoms. It is to be noted that the present refinement is based on the method as described in the section 3.2 and it differs from the previous report [62]. The maximum DMSDA value [$5 \times 10^{-4} \text{Å}^2$ for $O(1)-C(8)$ and $C(9)-C(4)$ bond] is within Hirshfeld's limit ($<10^{-3} \text{Å}^2$) of rigid bond test and almost featureless residual densities (-0.206, $0.347 \, e\text{Å}^{-3}$) with respect to the S-atom, indicating the good quality of the data and the multipole model. The lone-pair of electrons of the S-atom and the O-atom was clearly seen from the static and dynamic deformation density maps (not shown here), which also showed the accuracy in chemical bonding features of the molecule. The molecules in the crystal lattice are held together mainly *via* van der Waals interactions. However, based on the first four of the KP criteria three $C-H \cdots S$ interactions and only one $C-H \cdots O$ hydrogen bond were identified. Two $C-H \cdots S$ and the $C-H \cdots O$ interactions bring two molecules together to form a dimer as
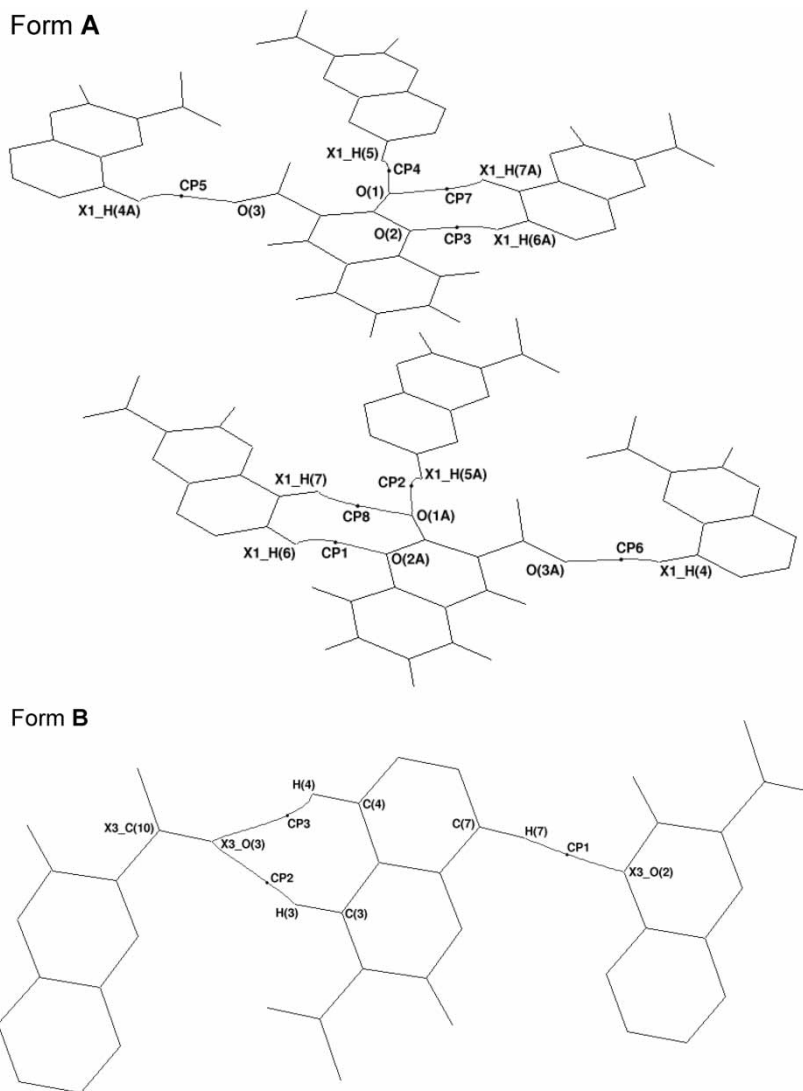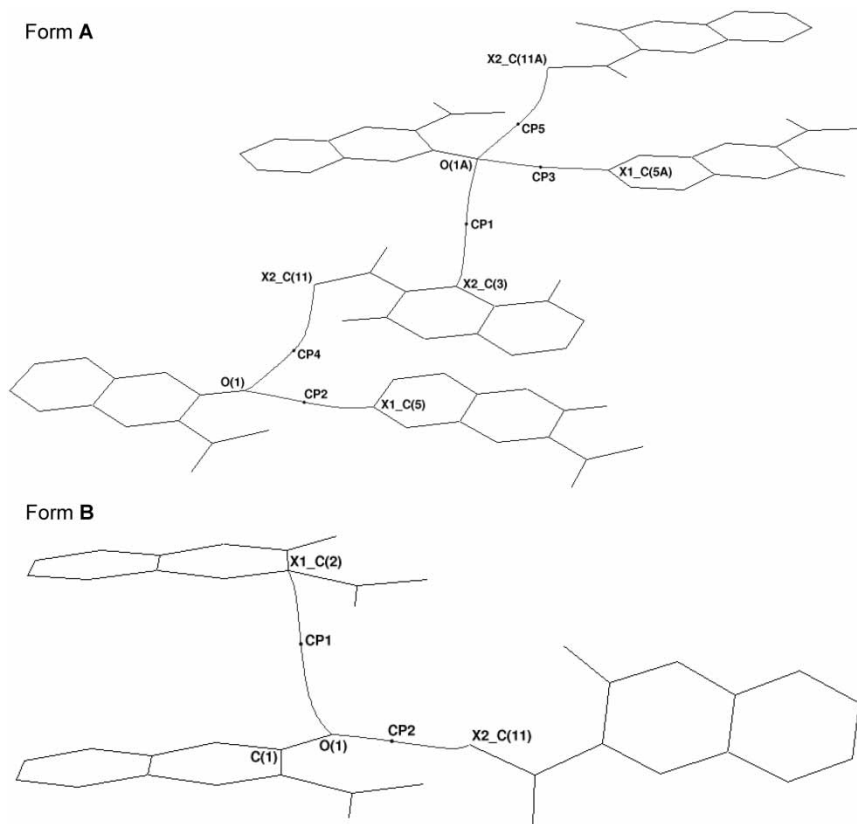
Figure 8. Bond path character in form **A** and form **B** of 3-acetylcoumarin showing the critical point locations along the $C-H \cdots O$ interaction lines shown in grey.

can be seen from the BP characteristic in figure 16. The Laplacian map (see figure 17) highlights one of the $C-H \cdots S$ interactions forming the dimer. Table 3 lists the dipole moments and once again it is observed to follow similar trends in terms of the value of the dipole moment (crystal dipole moment higher that the theoretically optimized single molecule).

5.2.5.   Dithiocoumarin (2H-thiochromene-2-thione) [125,126]**.** This disubstituted sulfur derivative of coumarin crystallizes in the centrosymmetric space group $P\bar{1}$.
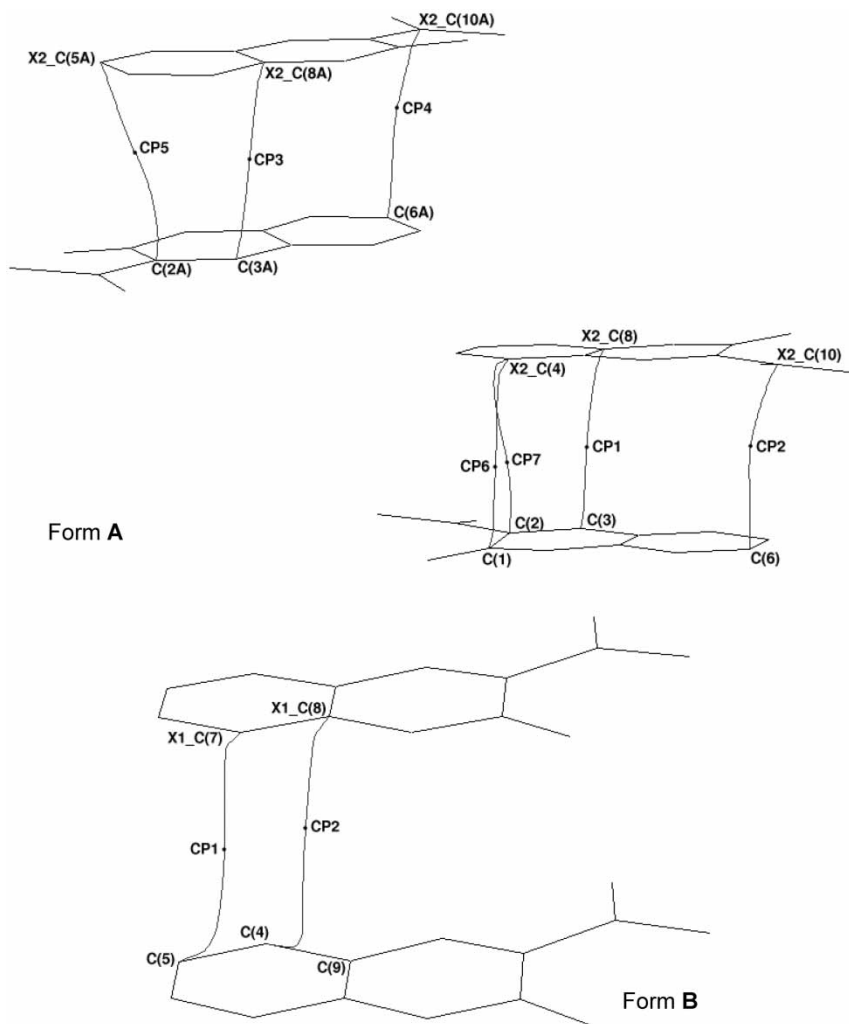
Figure 9. Bond path character in form **A** and form **B** of 3-acetylcoumarin showing the critical point locations along the $C_\pi \cdots C_\pi$ interaction lines.

The molecular structure along with the atom labeling for non-H-atoms is shown in figure 18. The details of experimental and theoretical charge density distributions on this compound will be discussed elsewhere [126]. Here we present only a few results in the context of charge-density distribution on sulfur containing molecules and the weak intermolecular interactions. The Laplacian maps (see figure 19) from experimental and theoretical charge density distributions show the nature of charge-density distribution in the vicinity of the S-atom and the arrangement of atoms inside the molecule. The molecules are held together in the crystal lattice *via* two $S \cdots S$ and two $C-H \cdots S$ weak interactions, which were identified based on the first four of the KP criteria. Figure 20 traces the $S \cdots S$ interactions in terms of BCPs and BPs *via* a center of symmetry between the two molecules, showing that a dimeric assembly

Figure 10. Bond path character in form **A** and form **B** of 3-acetylcoumarin showing the critical point locations along the C=O $\cdots$ C$_\pi$ interaction lines.
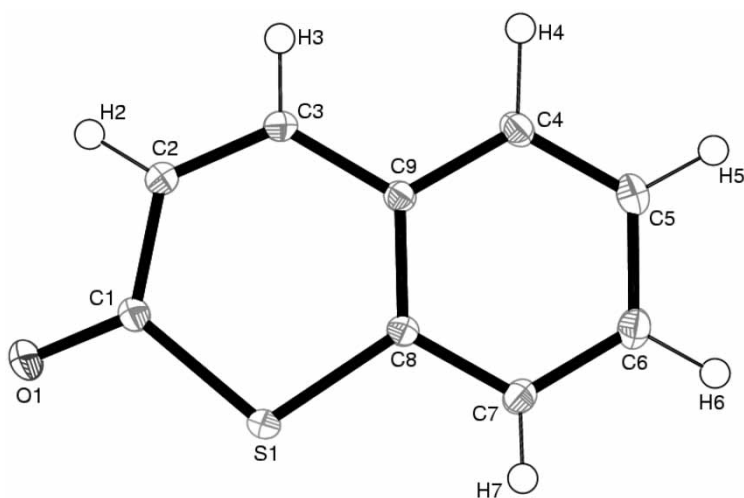
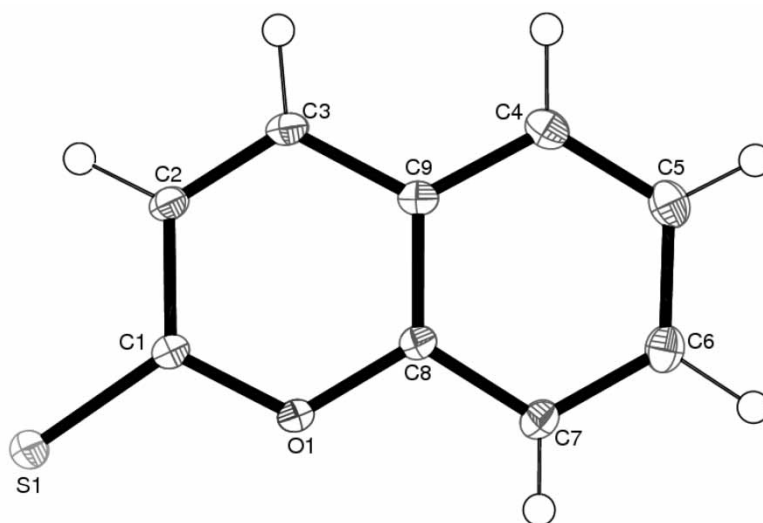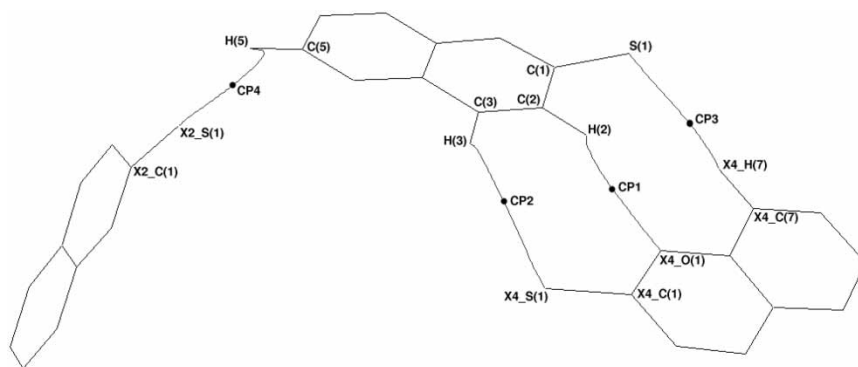Figure 11. ORTEP view with labels for atoms of 1-thiocoumarin at 90 K with 50% ellipsoid probability (non-H-atoms).
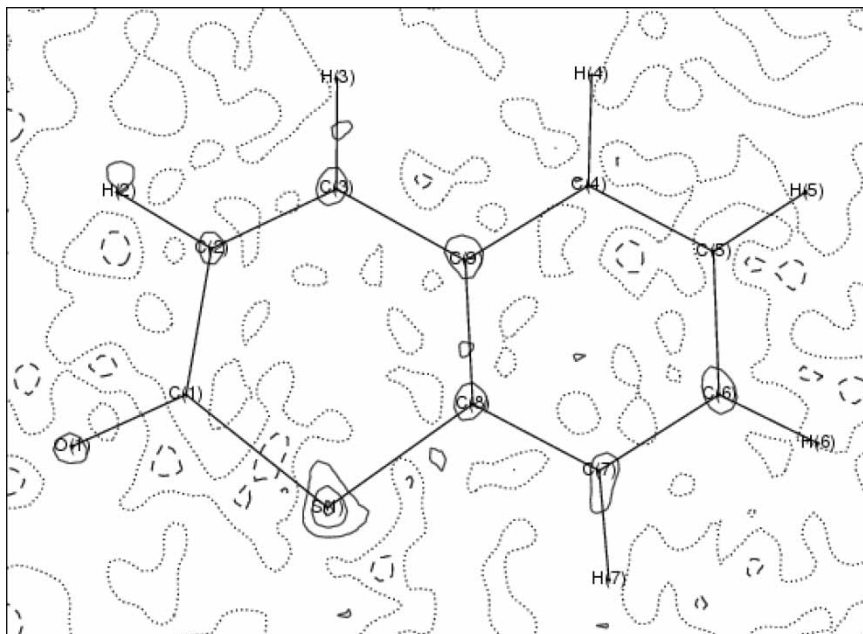
Figure 12.   Residual density map in the molecular plane of 1-thiocoumarin, for all residual density maps the positive (solid lines) and negative (broken lines) contour starts at $\pm 0.05\,e\text{Å}^{-3}$ and with the intervals of $\pm 0.1\,e\text{Å}^{-3}$, contour at zero is shown as dotted lines.

is brought through bifurcated contacts. The $S(2)\cdots S(2)$ contact is shorter ($R_{ij} = 3.429\,\text{Å}$, $\rho_b = 0.037\,e\text{Å}^{-1}$) than the $S(1)\cdots S(2)$ contact ($R_{ij} = 3.658\,\text{Å}$, $\rho_b = 0.029\,e\text{Å}^{-1}$) [127]. Further, the Laplacian map (see figure 21) shows the distribution of charge densities and the corresponding BCPs in this region. The nature of BPs along with the BCPs for $C-H\cdots S$ interactions is shown in figure 22.

### 5.3. *Evaluation of intermolecular interactions: limit of a hydrogen bond*

We have evaluated the nature of $C-H\cdots O$ and $C-H\cdots\pi$ interactions based on the experimental and theoretical charge density analysis on **coumarin**, **1-thiocoumarin**, and **3-acetylcoumarin (form A)** [30]. Only these three compounds show both $C-H\cdots O$ and $C-H\cdots\pi$ interactions concomitantly but not the other three of the structures as discussed above. The basic idea in choosing these two types of interactions is to allow the exploration of the region of the limit of a weak hydrogen bond as compared to a van der Waals interaction. Based on all **eight** of the KP criteria, for the first time, we have classified $C-H\cdots O$ interactions into two categories, hydrogen bonded and weak van der Waals interaction and $C-H\cdots\pi$ interactions as weak van der Waals interactions [30]. A total of 15 $C-H\cdots O$ interactions and 21 $C-H\cdots\pi$ interactions, in all 36 interactions, were selected from the three compounds. It has been observed that the intermolecular interactions follow an exponential dependence of electron density, ρ_b and energy densities [$V(r_{CP})$, $G(r_{CP})$, and $E(r_{CP})$] at the BCPs. Figure 23 shows the exponential dependence of ρ_b as a function of the length of the interaction line, R_{ij}. It is remarkable that even in this narrow range the dependence is analogous to Pauling's relation between bond orders and inter-nuclear
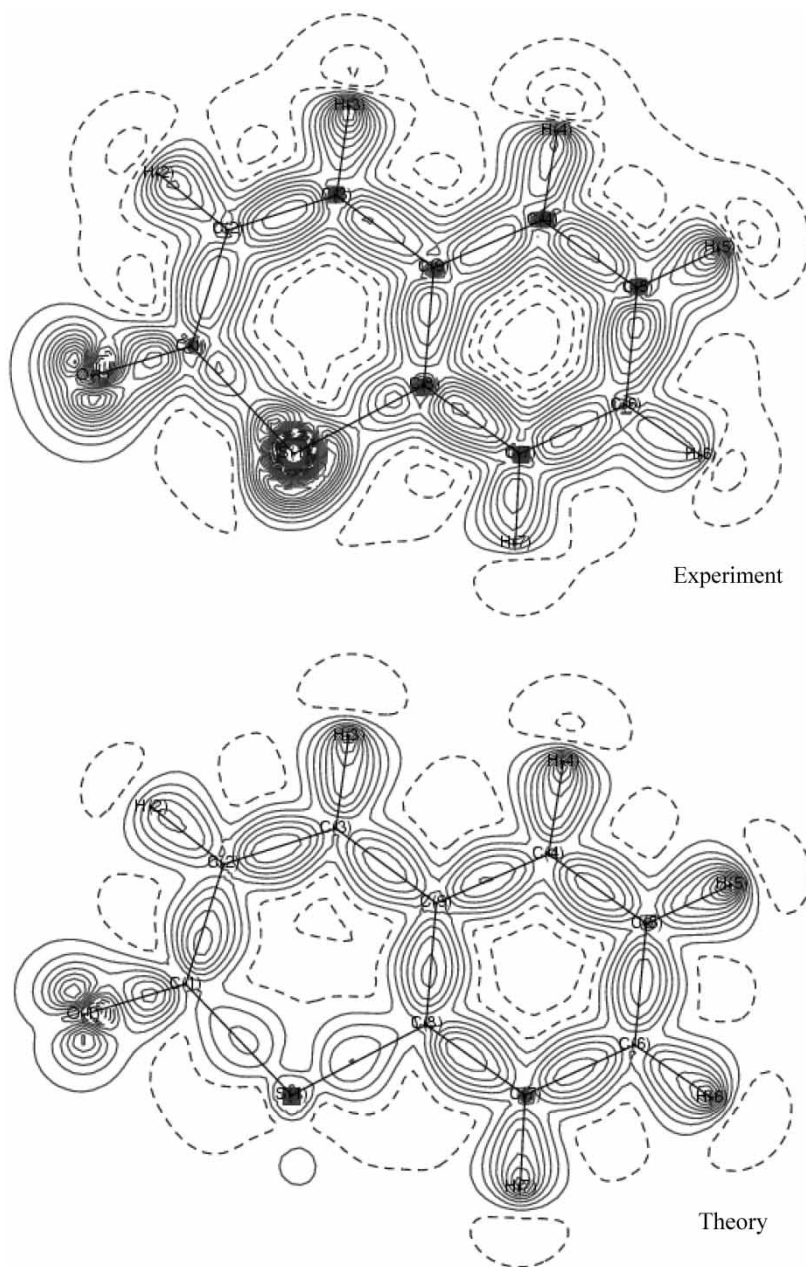
Figure 13.   Static deformation density maps (experimental and theoretical) for 1-thiocoumarin.

distances [128–131]. Most of the C−H⋯O hydrogen bonds reside in the range 2.4 to 2.7 Å for R_{ij}, while the C−H⋯π aggregates beyond 3 Å. Significantly, the shaded region in figure 23 between the R_{ij} values of 2.75 to 2.85 Å contain representative from both C−H⋯O and C−H⋯π contacts, which was defined as the '*region of overlap*' between the hydrogen-bond and an interaction. Both the local kinetic and the
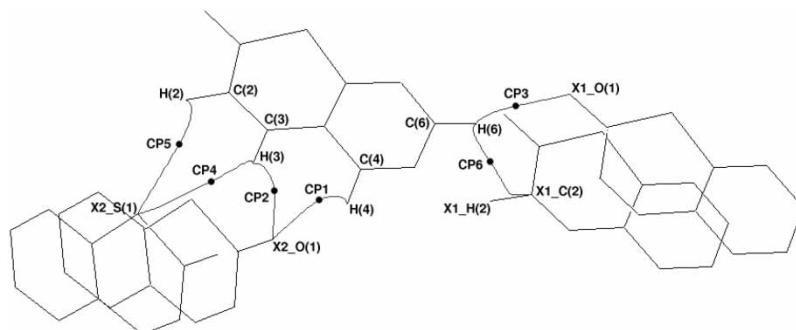
Figure 14. Bond path character in 1-thiocoumarin showing the critical point locations along the C−H···O, C−H···S, and C−H···C$_\pi$ interactions shown as dark dots.

Figure 15. ORTEP view with labels for atoms of 2-thiocoumarin at 90 K with 50% ellipsoid probability (non-H-atoms).
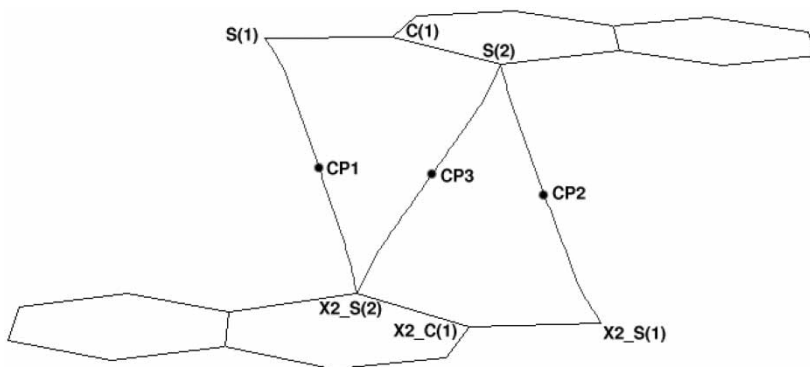

Figure 16. Bond path character in 2-thiocoumarin showing the critical point locations along the C−H···O and C−H···S interactions shown as dark dots.
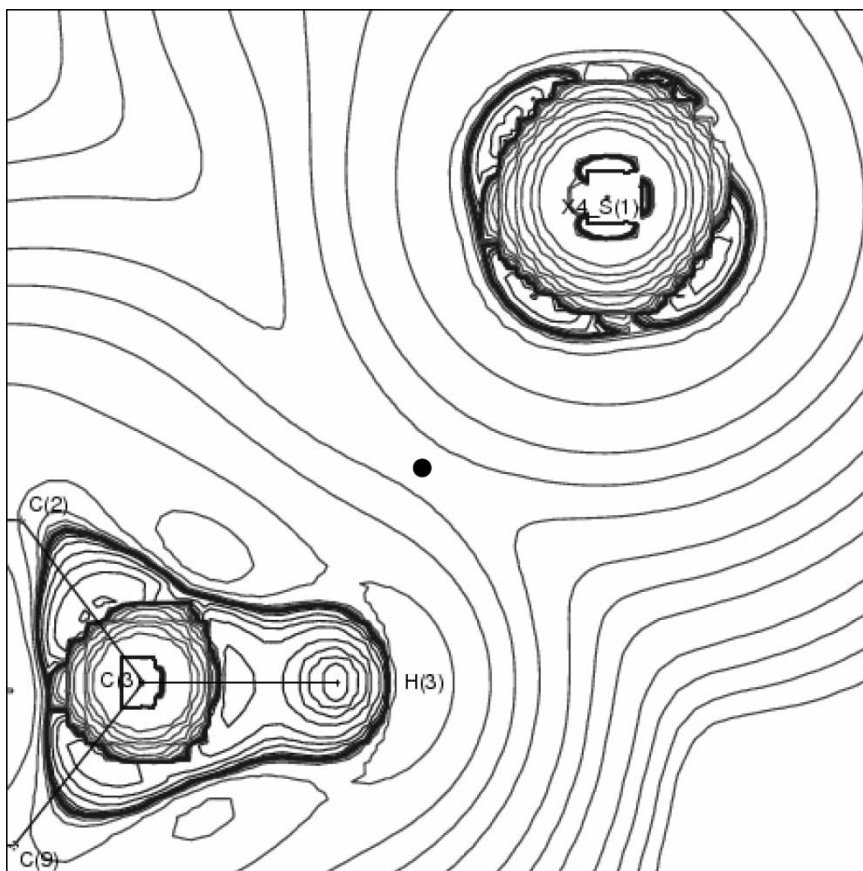
Figure 17. Laplacian $[\nabla^2 \rho_b(\mathbf{r})]$ of a representative $C-H \cdots S$ intermolecular interaction in 2-thiocoumarin.
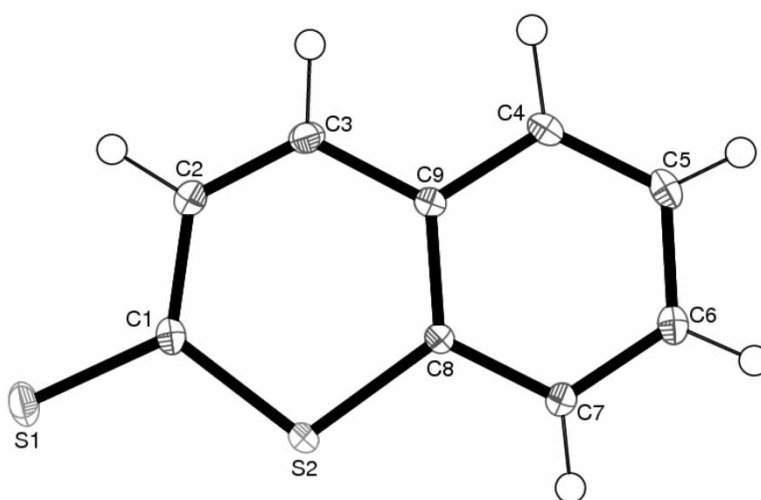
Figure 18. ORTEP view with labels for atoms of dithiocoumarin at $90\,K$ with 50% ellipsoid probability (non-H-atoms).
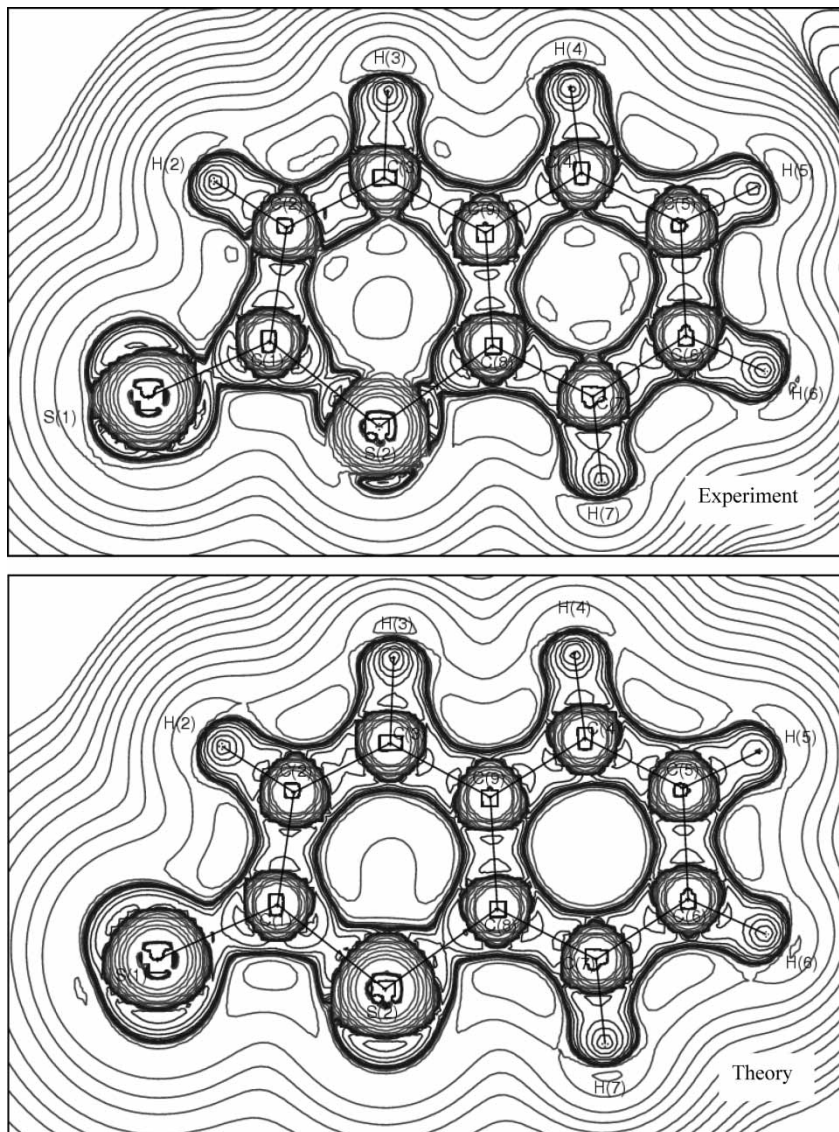
Figure 19. Laplacian [$\nabla^2 \rho_b(\mathbf{r})$] distribution (experimental and theoretical) in the plane of the molecule of dithiocoumarin.

potential energy densities [$G(r_{CP})$ and $V(r_{CP})$] and hence the total energy density [$E(r_{CP})$] at BCPs were calculated essentially to represent a quantity proportional to the hydrogen bond energy. Once again it is observed that the '*region of overlap*' deline-ates the hydrogen-bonding region with the interaction region as shown by the shaded area in figure 24. The relationship of the Laplacian ($\nabla^2 \rho_b$) and R_{ij} follows the 'Morse-like' dependence as can be seen from figure 25. In the distribution, the '*region of overlap*' is clearly marked in the range 2.75–2.85 Å in R_{ij} and the Laplacian lies in the range 0.35–0.55 eÅ^{-5}. The quantities $\Delta r_D + \Delta r_A$ and $\Delta r_D - \Delta r_A$ represent

Figure 20. Bond path character in dithiocoumarin showing the critical point locations along the S···S interactions shown as dark dots.
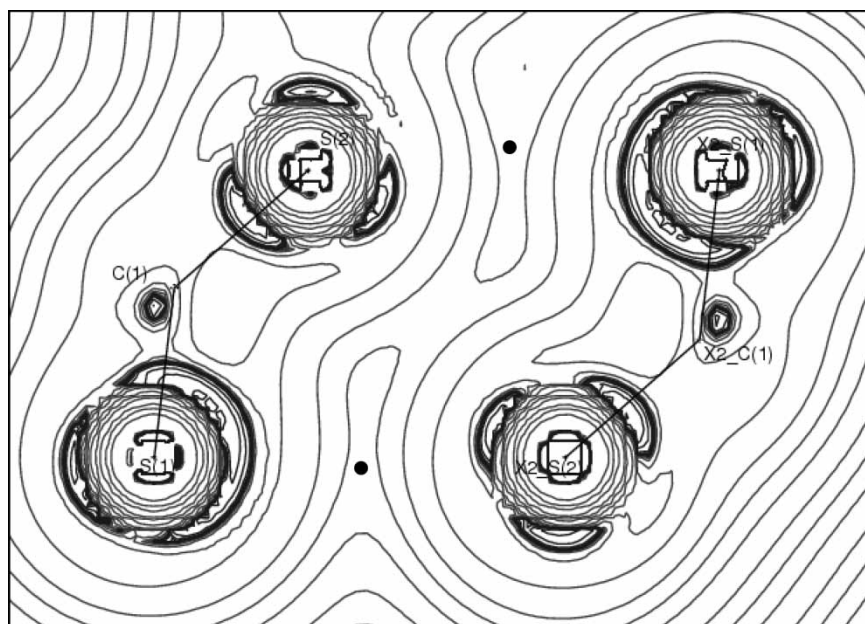
Figure 21. Laplacian [$\nabla^2 \rho_b(\mathbf{r})$] shows the S···S intermolecular interaction in dithiocoumarin.

the interpenetration of van der Waals spheres of the donor and acceptor atoms. Figure 26 shows the linear correlation between $\Delta r_D + \Delta r_A$ and R_{ij}, which shows the difference between C−H···O hydrogen bonds and C−H···π interactions; and the limit of the hydrogen bond is well defined with R_{ij} values between 2.75 and 2.85 Å for the '*region of overlap*'.

The evaluation of integrated properties over the basin of the H-atoms involved in the interactions also distinguishes these two types of interactions. The atomic properties such as, charge, potential energy, dipolar polarization, and volume of H-atoms involved in the C−H···O and C−H···π interactions were determined in the crystal
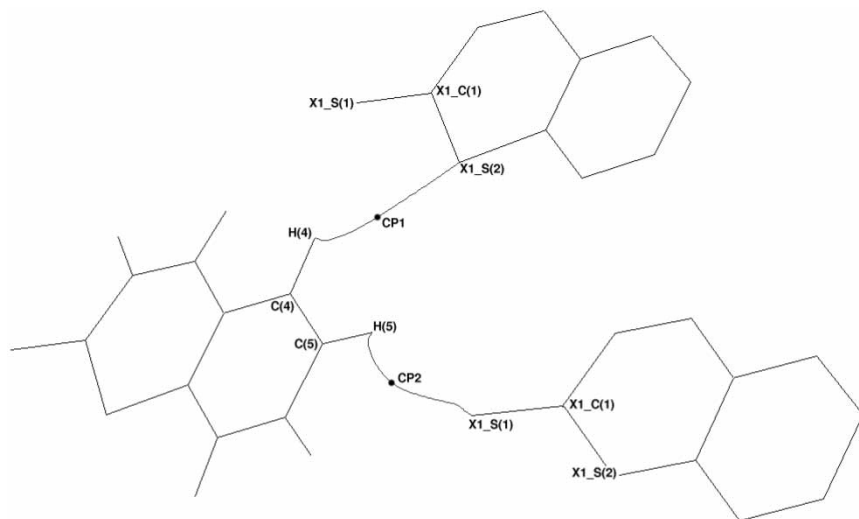
Figure 22.   Bond path character in dithiocoumarin showing the critical point locations along the C−H⋯S interactions.
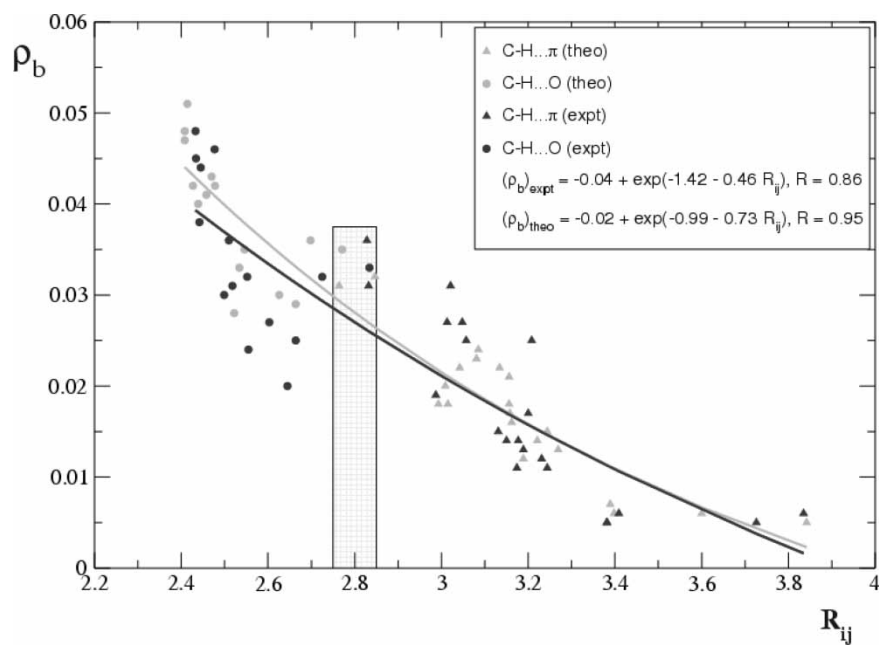
Figure 23.   Exponential dependence of ρ_b [eÅ^{-3}] on the interaction length R_{ij} [Å] for C−H⋯X (X=O or C$_\pi$) containing $N = 36$ data points. The points represent experimental and theoretical values respectively. The inset gives the details of the fitting models. The dark and light lines represent experimental and theoretical fitting, respectively, along with correlation coefficients R.
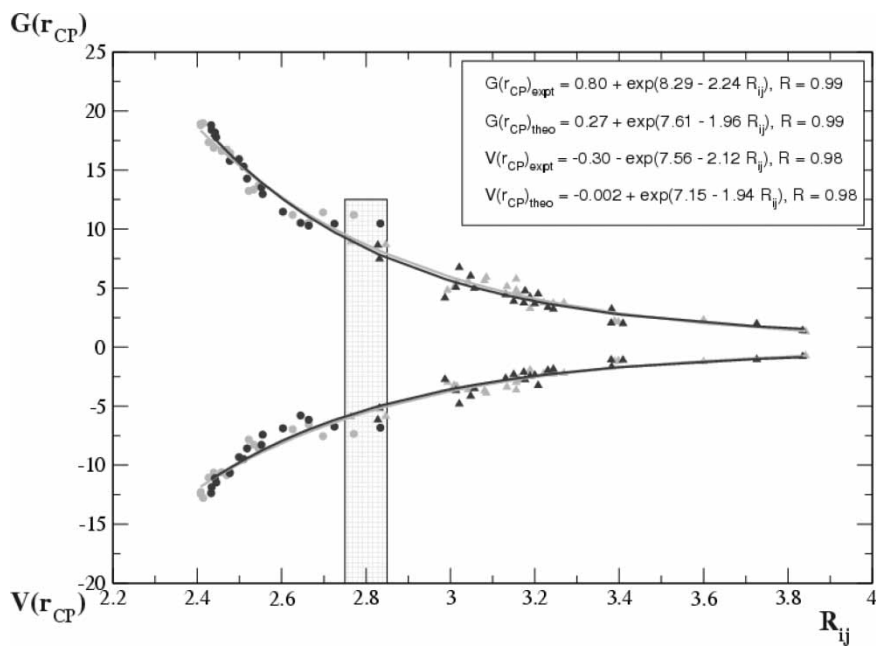
Figure 24. Exponential fitting of local potential energy density $V(r_{CP})$ [kJ mol^{-1}bohr^{-3}] and local kinetic energy density $G(r_{CP})$ [kJ mol^{-1}bohr^{-3}] values on R_{ij} [Å] for $N = 36$ data points.
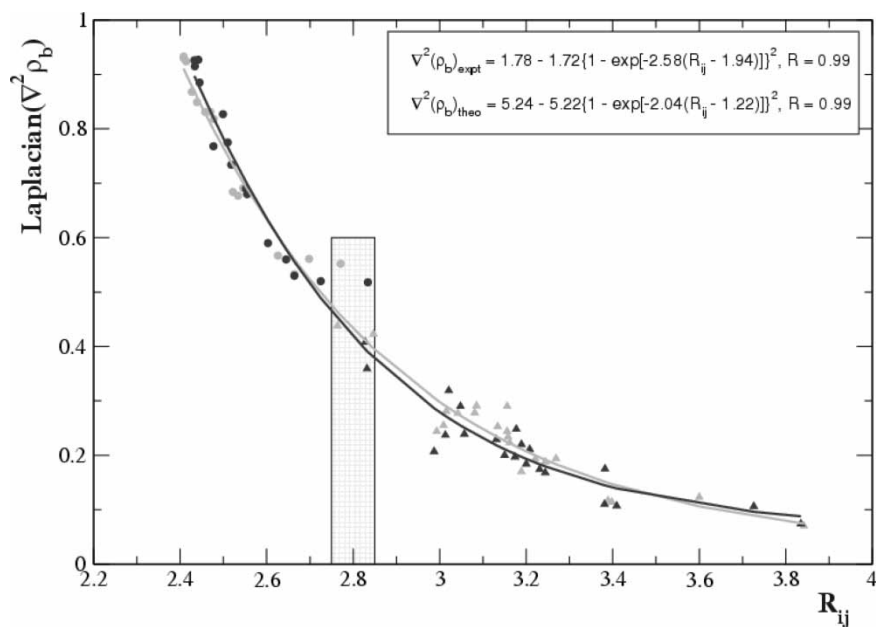
Figure 25. Morse-like dependence of Laplacian [$\nabla^2 \rho_b(\mathbf{r})$] (eÅ^{-5}) on R_{ij} [Å] for $N = 36$ data points.
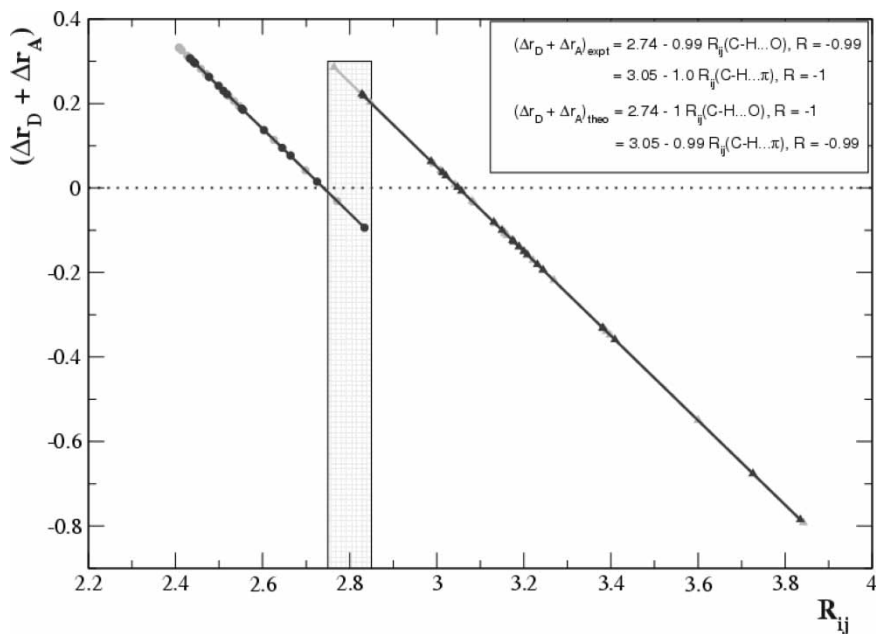
Figure 26. Linear dependence of $(\Delta r_D + \Delta r_A)$ [Å] on R_{ij} [Å] for $N=15$ (C−H$\cdots$O) and $N=21$ (C−H$\cdots$C$_\pi$) data points. The dotted line corresponds to $(\Delta r_D + \Delta r_A) = 0$.

(experimental and theoretical) and in the isolated molecule. A general trend emerges on inspection of the resulting values, the C−H$\cdots$O hydrogen bonds demarcate from the C−H$\cdots\pi$ van der Waals interactions, in terms of the atomic basin properties [30]. It has been noticed that a higher electron loss was found in the case of formation of a hydrogen bond and smaller electron loss reflects weak interaction. The differences in the potential energy (*PE*) in all cases depicted the expected trend, destabilizing the H-atom upon crystal formation. The trends show that the increase in the *PE* for C−H$\cdots$O hydrogen bond is larger compared to that in the C−H$\cdots\pi$ regime. The energy changes were strikingly significant in distinguishing between a C−H$\cdots$O hydrogen bond and a C−H$\cdots\pi$ interaction. A measure of the extent and direction of dipolar polarization of the atomic electron density is given by the magnitude of the first moment and these values decrease more in the case of a C−H$\cdots$O hydrogen bond than a C−H$\cdots\pi$ interaction. The decrease of H-atom's volume is quite significant to bring in the difference in bond strength between the two types of interactions and it follows the same trend as the previous one. All these observations put the distinguishing hydrogen bonding nature from that of the van der Waals interactions on a quantitative footing.

6. Concluding remarks

With the knowledge of molecular recognition and packing of molecules in a crystal lattice, the area of crystal engineering has evolved over three decades into maturity. However, until recently the impact was mainly superficial since the results were based

on qualitative interpretations in terms of distance and angle criteria. Even though the concept of synthons gained significant importance in the crystallographic literature, the lack of understanding of the nature of interactions in terms of the electron density had remained a lacuna. During the past decade, X-ray charge-density analysis has made significant progress with advances in technology and subsequently in experimental methods, together with developments in theoretical approaches on both isolated molecules and periodic crystals. The quality of experimental data has seen enormous improvement and hence investigation of more complex systems, involving weak intermolecular interactions, has come into the purview. As can be seen from the current review, very subtle but significant differences in interaction energies can be examined fairly accurately and comparisons can be drawn from theoretical evaluations. The methods of analysis, particularly in the case of weak intermolecular interactions, are becoming more and more accessible, so that in the next few years the applications may find relevance in complex chemical and biological systems.

Acknowledgement

References

[1] T.S. Koritsánszky, P. Coppens. *Chem. Rev.*, **101**(6), 1583 (2001).
[2] Y.A. Abramov, A. Volkov, G. Wu, P. Coppens. *Acta Cryst.*, **A56**, 585 (2000).
[3] S. Dahaoui, C. Jelsch, J.A.K. Howard, C. Lecomte. *Acta Cryst.*, **B55**, 226 (1999).
[4] A. Volkov, G. Wu, P. Coppens. *J. Synchrotron Rad.*, **6**, 1007 (1999).
[5] A. Martin, A.A. Pinkerton. *Acta Cryst.*, **B54**, 471 (1998).
[6] P. Coppens. *Acta Cryst.*, **A54**, 779 (1998).
[7] M.A. Spackman. *Annu. Rep. Prog. Chem., Sect. C: Phys. Chem.*, **94**, 177 (1997).
[8] M.A. Spackman, A.S.Brown. *Annu. Rep. Prog. Chem., Sect. C: Phys. Chem.*, **91**, 175 (1994).
[9] G.R. Desiraju. *Crystal Engineering: The Design of Organic Solids*, Elsevier, Amsterdam (1989).
[10] J.J. McKinnon, M.A. Spackman, A.S. Mitchell. *Acta Cryst.*, **B60**, 627 (2004).
[11] T. Koritsánszky, R. Flaig, D. Zobel, H.-G. Krane, W. Morgenroth, P. Luger. *Science*, **279**, 356 (1998).
[12] C. Katan, P. Rabiller, L. Toupet. *Acta Cryst.*, **A56**, s18 (2000).
[13] P. Coppens. *Phys. Rev. Lett.*, **35**, 98 (1995).
[14] N.K. Hansen, P. Coppens. *Acta Cryst.*, **A34**, 909 (1978).
[15] T.S. Koritsánszky, S. Howard, P. Macchi, C. Gatti, L.J. Farrugia, P.R. Mallinson, A. Volkov, Z. Su, T. Richter, N.K. Hansen. *XD*(version 4.10, July), A computer program package for multipole refinement and analysis of electron densities from diffraction data. Free University of Berlin, Germany; University of Wales, Cardiff, UK.; Università di Milano, U.K.; CNR-ISTM, Milano, U.K.; University of Glasgow, U.K.; State University of New York, Buffalo, USA.; University of Nancy, France (2003).

[16] M.J. Frisch, G.W. Trucks, H.B. Schlegel, G.E. Scuseria, M.A. Robb, J.R. Cheeseman, V.G. Zakrzewski, J.A. Montgomery Jr., R.E. Stratmann, J.C. Burant, S. Dapprich, J.M. Millam, A.D. Daniels, K.N. Kudin, M.C. Strain, O. Farkas, J. Tomasi, V. Barone, M. Cossi, R. Cammi, B. Mennucci, C. Pomelli, C. Adamo, S. Clifford, J.W. Ochterski, G.A. Petersson, P.Y. Ayala, Q. Cui, K. Morokuma, D.K. Malick, A.D. Rabuck, K. Raghavachari, J.B. Foresman, J. Cioslowski, J.V. Ortiz, B.B. Stefanov, G. Liu, A. Liashenko, P. Piskorz, I. Komaromi, R. Gomperts, R.L. Martin, D.J. Fox, T. Keith, M.A. Al-Laham, C.Y. Peng, A. Nanayakkara, A. Gonzalez, M. Challacombe, P.M.W. Gill, B. Johnson, W. Chen, M.W. Wong, J.L. Andres, C. Gonzalez, M. Head-Gordon, E.S. Replogle, J.A. Pople. *GAUSSIAN 98*, Gaussian, Inc., Pittsburgh, PA (1998).
[17] V.R. Saunders, R. Dovesi, C. Roetti, R. Orlando, C.M. Zicovich-Wilson, N.M. Harrison, K. Doll, B. Civalleri, I. Bush, Ph. D'Arco, M. Llunell. *CRYSTAL2003* User's Manual, University of Torino, Torino (2003).
[18] R.F.W. Bader. *Atoms in Molecules-A Quantum Theory*, Clarendon, Oxford (1990).
[19] R.F.W. Bader. *J. Phys. Chem.*, **A102**, 7314 (1998).
[20] U. Koch, P.L.A. Popelier. *J. Phys. Chem.*, **99**, 9747 (1995).
[21] P.L.A. Popelier. *Atoms in Molecules. An Introduction*, pp. 150–153, Prentice Hall, UK (2000).
[22] F.H. Allen. *Acta Cryst.*, **B58**, 380 (2002).
[23] F.H. Allen, W.D.S. Motherwell. *Acta Cryst.*, **B58**, 407 (2002).
[24] G.R. Desiraju. *Angew. Chem. Int. Ed. Engl.*, **34**, 2311 (1995).
[25] G.R. Desiraju. *Chem. Commun.*, **16**, 1475 (1997).
[26] A. Nangia, G.R. Desiraju. *Design of Organic Solids*, E. Weber (Ed.), pp. 57–95, Springer-Verlag, Berlin (1998).
[27] T. Steiner. *Cryst. Rev.*, **9**(2–3), 177 (2003).
[28] G.R. Desiraju, T. Steiner. *The Weak Hydrogen Bonds: In Structural Chemistry and Biology*, Oxford University Press, Oxford, New York (1999).
[29] C.B. Aakeröy, T.A. Evans, K.R. Seddon, I. Pálinkó. *New J. Chem.*, **23**, 145 (1999).
[30] P. Munshi, T.N. Guru Row. *J. Phys. Chem.*, **A109**, 659 (2005).
[31] M.C. Etter. *Acc. Chem. Res.*, **23**, 120 (1990).
[32] F.H. Allen, O. Kennard, D.G. Watson. Crystallographic database: search and retrieval of information from the Cambridge structural database. In *Structure Correlation*, H.-B. Bürgi, J.D. Dunitz (Eds), Vol. 1, pp. 71–110, VCH, Weinheim (1994).
[33] R. Taylor, F.H. Allen. Statistical and numerical methods of data analysis. In *Structure Correlation*, H.-B. Bürgi, J.D. Dunitz (Eds), Vol. 1, pp. 111–161, VCH, Weinheim (1994).
[34] P. Coppens, T.N. Guru Row, P. Leung, E.D. Stevens, P.J. Becker, Y.W. Yang. *Acta Cryst.*, **A35**, 63 (1979).
[35] F.L. Hirshfeld. *Acta Cryst.*, **B27**, 769 (1971).
[36] R.F. Stewart. *Acta Cryst.*, **A32**, 565 (1976).
[37] P. Coppens. *X-ray Charge Densities and Chemical Bonding*, Oxford University Press, Oxford (1997).
[38] T.N. Guru Row. *Coord. Chem. Rev.*, **183**, 81 (1999).
[39] J. Bernstein, M.C. Etter, L. Leiserowitz. The role of hydrogen bonding in molecular assemblies. In *Structure Correlation*, H.-B. Bürgi, J.D. Dunitz (Eds), Vol. 2, pp. 431–507, VCH, Weinheim (1994).
[40] G.A. Jeffrey. *Cryst. Rev.*, **9**, 135 (2003).
[41] R. Taylor, O. Kennard. *J. Am. Chem. Soc.*, **104**, 5063 (1982).
[42] L. Shimoni, H.L. Carrell, J.P. Glusker, M.M. Coombs. *J. Am. Chem. Soc.*, **116**, 8162 (1994).
[43] A.R. Choudhury, T.N. Guru Row. *Cryst. Growth Des.*, **4**, 47 (2004).
[44] M. Iwaoka, S. Tomoda. *J. Am. Chem. Soc.*, **116**, 4463 (1994).
[45] P.R. Mallinson, G.T. Smith, C.C. Wilson, E. Grech, K. Woźniak. *J. Am. Chem. Soc.*, **125**, 4259 (2003).
[46] G.C. Pimentel, A.L. McClellan. *The Hydrogen Bond*, Freeman, San Francisco (1960).
[47] A. Wagner, R. Flaig, B. Dittrich, H. Schmidt, T. Koritsánszky, P. Luger. *Chem. Eur. J.*, **10**, 2977 (2004).
[48] D. Leusser, J. Henn, N. Kocher, B. Engels, D. Stalke. *J. Am. Chem. Soc.*, **126**, 1781 (2004).
[49] J.W. Bats, P. Coppens. *Acta Cryst.*, **B33**, 37 (1977).
[50] J.W. Bats, P. Coppens, Å. Kvick. *Acta Cryst.*, **B33**, 1534 (1977).
[51] J.W. Bats, P. Coppens, T.F. Koetzle. *Acta Cryst.*, **B33**, 1542 (1977).
[52] H.P. Weber, B.M. Carven. *Acta Cryst.*, **B43**, 202 (1987).
[53] B. Fabius, C. Cohen-Addad, F.K. Larsen, M.S. Lehmann, P. Becker. *J. Am. Chem. Soc.*, **111**, 5728 (1989).
[54] B.N. Figgis, B.B. Iversen, F.K. Larsen, P.A. Reynolds. *Acta Cryst.*, **B49**, 794 (1993).
[55] K.L. McCormack, P.R. Mallinson, B.C. Webster, D.S. Yufit. *J. Chem. Soc. Faraday Trans.*, **92**, 1709 (1996).
[56] E. Espinosa, E. Molins, C. Lecomte. *Phys. Rev. B*, **56**, 1820 (1997).
[57] S. Dahaoui, V. Pichon-Pesme, J.A.K. Howard, C. Lecomte. *J. Phys. Chem.*, **A103**, 6240 (1999).
[58] W. Scherer, M. Spiegler, B. Pedersen, M. Tafipolsky, W. Heiringer, B. Reinhard, A.J. Downs, S. McGrady. *Chem. Commun.*, **7**, 635 (2000).
[59] S. Pillet, M. Souhassou, Y. Pontillon, A. Caneschi, D. Gatteschi, C. Lecomte. *New J. Chem.*, **25**, 131 (2001).

[60] T.W. Hambley, D.E. Hibbs, P. Turner, S.T. Howard, M.B. Hursthouse. *J. Chem. Soc. Perkin Trans.*, **2**, 235 (2002).
[61] D. Leusser, B. Walfort, D. Stalke. *Angew. Chem. Int. Ed. Engl.*, **12**, 2079 (2002).
[62] (a) P. Munshi, T.N. Guru Row. *Acta Cryst.*, **B58**, 1011 (2002). (b) P. Munshi, T.N. Guru Row. *Acta Cryst.*, **B59**, 159 (2003).
[63] D.E. Hibbs, C.J. Austin-Woods, J.A. Platts, J. Overgaard, P. Turner. *Chem. Eur. J.*, **9**(5), 1075 (2003).
[64] J. Overgaard, D.E. Hibbs. *Acta Cryst.*, **A60**, 480 (2004).
[65] C.-R. Lee, T.-H. Tang, L. Chen, C.-C. Wang, Y. Wang. *J. Phys. Chem. Sol.*, **65**, 1957 (2004).
[66] M.A. Spackman. *Chem. Rev.*, **92**, 1769 (1992).
[67] P. Seiler. *Accurate Molecular Structures. Their Determination and Importance*, A. Domenicano, I. Hargittai (Eds), p. 170, Oxford University Press, Oxford (1992).
[68] Bruker. *SMART* (V5.628), *SAINT* (V6.45a)., Bruker AXS Inc., Madison, Wisconsin, USA (2004).
[69] R.H. Blessing. *Cryst. Rev.*, **1**, 3 (1987).
[70] G.M. Sheldrick. *SHELXS97* and *SHELXL97*. Program for crystal structure refinement. University of Göttingen, Germany (1997).
[71] L.J. Farrugia. *J. Appl. Cryst.*, **32**, 837 (1999).
[72] L.J. Farrugia. *J. Appl. Cryst.*, **30**, 565 (1997).
[73] R.F. Stewart, M.A. Spackman. *Valray User's Manual*, Department of Chemistry, Carnegie-Mellon University, Pittsburgh, PA (1983).
[74] B.M. Craven, H.P. Weber, X. He. *Technical Report TR-872*, Department of Crystallography, University of Pittsburgh, Pittsburgh, PA (1987).
[75] B.N. Figgis, P.A. Reynolds, G.A. Williams. *J. Chem. Soc., Dalton Trans.*, **12**, 2339 (1980).
[76] P. Munshi, T.N. Guru Row. *J. Phys. Chem. A* (submitted) (2005).
[77] F.H. Allen. *Acta Cryst.*, **B42**, 515 (1986).
[78] A.J.C. Wilson. *International Tables for Crystallography*, Vol. C, pp. 206–222, Kluwer Academic Publishers, Dordrecht (1992).
[79] E. Clementi, C. Roetti. *Atomic Data and Nuclear Data Tables*, **14**, 177 (1974).
[80] A. Volkov, C. Gatti, Yu. Abramov, P. Coppens. *Acta Cryst.*, **A56**, 252 (2002).
[81] Z. Kisiel, *PROSPE:* Programs for ROtational SPEctroscopy, available from http://info.ifpan.edu.pl/~kisiel/prospe.htm.
[82] M.A. Spackman. *J. Chem. Phys.*, **85**, 6579 (1986).
[83] Yu.A. Abramov, A. Volkov, G. Wu, P. Coppens. *J. Phys. Chem.*, **B104**, 2183 (2000).
[84] C. Gatti, V.R. Saunders, C. Roetti. *J. Chem. Phys.*, **101**, 10686 (1994).
[85] E. May, R. Destro, C. Gatti. *J. Am. Chem. Soc.*, **123**, 12248 and references therein (2001).
[86] R.S. Gopalan, G.U. Kulkarni, C.N.R. Rao. *Chem. Phys. Chem.*, **1**, 127 (2000).
[87] J.M. Cole, R.C.B. Copley, G.J. McIntyre, J.A.K. Howard, M. Szablewski, G.H. Cross. *Phys. Rev. B*, **65**, 125107 (2002).
[88] J.M. Cole, A.E. Goeta, J.A.K. Howard, G.J. McIntyre. *Acta Cryst.*, **B58**, 690 (2002).
[89] A.D. Becke. *J. Chem. Phys.*, **98**, 5648 (1993).
[90] C. Lee, W. Yang, R.G. Parr. *Phys. Rev. B*, **37**, 785 (1988).
[91] P.C. Hariharan, J.A. Pople. *Theor. Chim. Acta*, **28**, 213 (1973).
[92] M.A. Spackman, A.S. Mitchell. *Phys. Chem. Chem. Phys.*, **3**, 1518 (2001).
[93] S.F. Boys, F. Bernardi. *Mol. Phys.*, **19**, 553 (1970).
[94] J. Oddershede, S. Larsen. *J. Phys. Chem.*, **A108**, 1057 (2004).
[95] M.F. Guest, V.R. Saunders. *Mol. Phys.*, **28**, 819 (1974).
[96] E. Clementi. *Modern Techniques in Computational Chemistry: MOTECC 91*, *ESCOM*, Leiden (1991).
[97] F.M. Aicken, P.L.A. Popelier. *Can. J. Chem.*, **78**, 415 (2000).
[98] *MORPHY98*. A program written by P.L.A. Popelier with a contribution from R.G.A. Bone, UMIST, Manchester, U.K., EU (1998).
[99] P.L.A. Popelier. *J. Phys. Chem.*, **A102**, 1873 (1998).
[100] Yu.A. Abramov. *Acta Cryst.*, **A53**, 264 (1997).
[101] E. Espinosa, E. Molins, C. Lecomte. *Chem. Phys. Lett.*, **285**, 170 (1998).
[102] A. Bondi. *J. Phys. Chem.*, **68**, 441 (1964).
[103] S.C. Nyburg, C.H. Faerman. *Acta Cryst.*, **B41**, 274 (1985).
[104] K. Vishnumurthy, T.N. Guru Row, K. Venkatesan. Observations of the photochemical behavior of coumarins and related systems in the crystalline state. Understanding and manipulation excited-state processes. In *Molecular and Supramolecular Photochemistry*, V. Ramamurthy, K.S. Schanze (Eds), Vol. 8, pp. 427–460, Marcel Dekker Inc., New York, Basel (2001).
[105] D.C. Hooper, J.S. Wolfson, G.L. McHugh, M.B. Winters, M.N. Swartz. *Antimicrob. Agents Chemother.*, **22**, 662 (1982).
[106] A. Morris, A.D. Russell. *Prog. Med. Chem.*, **8**, 39 (1971).
[107] N.A. Nemkovich, H. Reis, W. Baumann. *Journal of Luminescence*, **71**, 255 and the references therein (1997).
[108] H. Khalfan, R. Abuknesha, M. Rond-Weaver, R.G. Price, R. Robinson. *Histochem. J.*, **18**, 497 (1986).

[109] J.P. Jasinski, E.S. Paight. *Acta Cryst.*, **C50**, 1928 (1994).
[110] J.P. Jasinski, R.C. Woudenberg. *Acta Cryst.*, **C51**, 107 (1995).
[111] B.-C. Yip, F.-M. Moo, K.-S. Lok, H.-K. Fun, K.A. Sivakumar. *Acta Cryst.*, **C52**, 477 (1996).
[112] T. Honda, I. Fujii, N. Hirayama, N. Aoyama, A. Miike. *Acta Cryst.*, **C52**, 395 (1996).
[113] J. Narasimha Moorthy, K. Venkatesan. *Bull. Chem. Soc. Jpn*, **67**, 1 (1994).
[114] K. Vishnumurthy, T.N. Guru Row, K. Venkatesan. *Photochem. Photobiol. Sci.*, **1**, 799 (2002).
[115] P. Munshi, K.N. Venugopala, B.S. Jayashree, T.N. Guru Row. *Cryst. Growth Des.*, **4**(6), 1105 (2004).
[116] J. Bernstein. *Polymorphism in Molecular Crystals*, Oxford University Press, Oxford, Great Britain (2002).
[117] J.M. Domagala, S.E. Hagen, E.T. Lunney, D. Bradly. Warner-Lambert Co. USA, US Patent No. 5510375, **A23** (1996).
[118] A.I. Eid, F.A. Ragab, S.L. El-Ansary, S.M. El-Gazayerly, F.E. Mourad. *Arch. Pharm.*, **327**, 211 (1994).
[119] J.E.F. Reynolds. *Martindale: The Extra Pharmacopoeia*, 30th Edn., The Pharmaceutical Press, London (1993).
[120] P. Munshi, T.N. Guru Row. *Acta Cryst.*, **E57**, o1175 (2001).
[121] P. Munshi, T.N. Guru Row. *Acta Cryst.*, **E58**, o353 (2002).
[122] F.L. Hirshfeld. *Acta Cryst.*, **A32**, 239 (1976).
[123] J. Bernstein, R.J. Davey, J.-O. Henck. *Angew. Chem. Int. Ed.*, **38**, 3440 (1999).
[124] V.S.S. Kumar, A. Addlagatta, A. Nangia, W.T. Robinson, C.K. Broder, R. Mondal, I.R. Evans, J.A.K. Howard, F.H. Allen. *Angew. Chem. Int. Ed.*, **41**, 3848 (2002).
[125] P. Munshi, T.N. Guru Row. *Acta Cryst.*, **E60**, o2168 (2004).
[126] P. Munshi, T.N. Guru Row. (submitted) (2005).
[127] T.N. Guru Row. R. Parthasarthy. *J. Am. Chem. Soc.*, **103**, 477 (1981).
[128] L. Pauling. *The Nature of the Chemical Bond*, Cornell University Press, Ithaca, New York (1960).
[129] P.R. Mallinson, K. Wozniak, G.T. Smith, K.L. McCormac. *J. Am. Chem. Soc.*, **119**, 11502 (1997).
[130] E. Espinosa, M. Souhassou, H. Lachekar, C. Lecomte. *Acta Cryst.*, **B55**, 563 (1999).
[131] E. Espinosa, I. Alkorta, J. Elguero, Molins. *J. Chem. Phys.*, **117**, 5529 (2002).

Subject index